Journal of Thermal Stresses
Publication details, including instructions for authors and subscription information:
http://www.tandfonline.com/loi/uths20

Coupled Thermo-Electro-Mechanical Analysis of Smart Plates Embedding Composite and Piezoelectric Layers

S. Brischetto [a] & E. Carrera [a]
[a] Department of Mechanical and Aerospace Engineering, Politecnico di Torino, Italy
Version of record first published: 30 Jul 2012.

To cite this article: S. Brischetto & E. Carrera (2012): Coupled Thermo-Electro-Mechanical Analysis of Smart Plates Embedding Composite and Piezoelectric Layers, Journal of Thermal Stresses, 35:9, 766-804

To link to this article: http://dx.doi.org/10.1080/01495739.2012.689232

Journal of Thermal Stresses, 35: 766–804, 2012

ISSN: 0149-5739 print/1521-074X online
DOI: 10.1080/01495739.2012.689232

Taylor & Francis
Taylor & Francis Group

COUPLED THERMO-ELECTRO-MECHANICAL ANALYSIS OF SMART PLATES EMBEDDING COMPOSITE AND PIEZOELECTRIC LAYERS

S. Brischetto and E. Carrera
Department of Mechanical and Aerospace Engineering, Politecnico di Torino, Italy

This article considers the static analysis of multilayered piezoelectric plates subjected to mechanical pressures and to field loads such as electric potential and temperature. The Principle of Virtual Displacements has been extended to thermo-electro-mechanical cases by including the virtual internal electric and thermal works and by writing the opportune constitutive relations. The governing equations are given in terms of three main primary variables (displacements, electric potential and temperature) and they are solved in a closed-form solution. The primary variables are expanded in the thickness direction in both Equivalent Single Layer (ESL) and Layer-Wise (LW) form with higher orders of expansion. The models proposed enable to obtain a quasi-3D description of the static thermo-electro-mechanical analysis of multilayered plates and to analyze the effects of each physical field involved. The limitations of classical theories for such analyses have also been discussed.

Keywords: Field loads; Layer wise approach; Multifield effects; Multilayered plates; Piezoelectric layers; Refined models.

INTRODUCTION

The next generation of aircraft and spacecraft could be manufactured as multilayered structures under the action of a combination of two or more physical fields. Examples of multifield analysis for multilayered structures are the so-called "smart structures", they can be considered as multilayered composite plates or shells with embedded piezoelectric layers which are used as sensors or actuators to develop electric fields that are able to counteract thermo-mechanical deformations [1]. Smart structures involve interactions between mechanical, thermal and electrical fields. Electrical and thermal loadings are "field loadings," which require the use of refined structural models, these last are also fundamental in layered structures with several interfaces. Interfaces lead to discontinuous distributions of thermal, electrical and mechanical properties along the thickness [2]. In [3], it has been demonstrated how the effect of the temperature field on the deformation field is not a one-way phenomenon, which means that a deformation of the body also produces changes in

Received 24 October 2011; accepted 19 February 2012.
Address correspondence to Salvatore Brischetto, Department of Mechanical and Aerospace Engineering, Politecnico di Torino, Corso Duca degli Abruzzi, 24, Torino 10129, Italy; E-mail: salvatore.brischetto@polito.it

its temperature. These features demonstrate that the mechanical and thermal aspects are coupled and inseparable as suggested in Nowinski's book [4]. The thermoelastic problem, where the temperature and deformation fields are decoupled, is defined as a partially coupled thermo-mechanical problem, on the contrary a fully coupled thermoelastic analysis has both temperature and displacements as primary variables in the thermo-mechanical governing equations [3].

In the present work the concept of fully coupled thermoelastic analysis has been extended to smart structures by considering the coupling between the thermal and mechanical fields and between the thermal and electrical fields. The electro-mechanical coupling, typical of smart structures with embedded piezoelectric layers, has extensively been investigated in past authors' works [5, 6]. In this paper a three-field analysis will be proposed, it will allow to investigate smart structures subjected to different loadings such as mechanical, electrical and thermal ones and to evaluate the weight and importance of the different coupling effects between the three physical fields involved. Altay and Dökmeci [7] have given the constitutive equations for a thermopiezoelectric medium and the extension of the Principle of Virtual Displacements to thermopiezoelectricity case, the main limitation of this work is the absence of assessments and benchmarks. Important suggestions about the thermo-mechanical coupling (electrical field is not included) have been given in [8] and [9]. The present article has two main aims: it gives a full coupling between mechanical, thermal and electrical fields which allows to discuss the importance of multifield effects and to analyze structures subjected to mechanical and field loadings; and, it gives refined multifield two-dimensional models which overcome the main limitations typical of classical theories when applied to such problems (see theories based on Kirchhoff [10] or Reissner/Mindlin [11, 12] hypotheses).

The importance of these topics is confirmed by the considerable amount of works proposed in the open literature. Chen et al. [13] have given the three-dimensional equations of transversely isotropic magneto-electro-thermo-elasticity, the temperature has not been completely coupled in the proposed equations because it has separately been solved by using the Fourier equation (steady heat conduction equation), no numerical results have been proposed. Pérez-Fernández et al. [14] have proposed 16 different types of constitutive relations of the linear thermo-magneto-electro-elasticity derived following the analytical formulation of solids thermodynamics. Such coupled effects represent the link between Newton equation of motion, Maxwell equations of electromagnetism and the heat equation. Liu and Zhang [15] have deduced the generalized Hamilton variational formulation of piezothermoelasticity and corresponding non-homogeneous Hamilton canonical equation, the isoparametric element formulation has enabled to analyze problems of hybrid plates with complicated geometries, boundary conditions and surface loads.

A full coupling for both constitutive and equilibrium equations has been proposed but no results for electrical loads have been given. Further applications, which are not directly connected with the structural multifield analysis of smart structures, are proposed in the following papers to remark about the capability of such a topic. The proposed constitutive model by Kim [16] has been employed to calculate the responses of ferroelectric polycrystal subjected to electric field and mechanical stress loading in several temperature conditions, the results have qualitatively been compared with experimental observations available in literature. Kumar and Chakraborty [17] have proposed a micromechanical model based on

strength of materials approach for evaluation of coupled thermo-electromechanical coefficients of piezoelectric fiber reinforced composites.

Rectangular representative volume element (RVE) with rectangular fibers has been considered and dependencies of effective coupled thermo-electro-mechanical coefficients on fiber volume fraction have been studied. Sakthivel and Arockiarajan [18] have proposed a model capable of predicting the effective properties of the composites subjected to thermo-electro-mechanical loading conditions. The outcome of this study has demonstrated the influence of thermal effect on the polarization in the composite even if constitutive equations have only a partial coupling for the thermal field.

The same authors have developed a micromechanics-based analytical model to evaluate the performance of 1-3-2 piezoelectric composite where both matrix and fiber materials have piezoelectrically been activated [19]. The proposed model was capable of predicting the effective properties of the composite subjected to thermoelectromechanical loading conditions. As in [18] the temperature was only partially coupled in constitutive equations. Yang et al. [20] have presented a set of basic equations, a variational principle and a finite element procedure to investigate the coupled behavior of thermo-electro-chemo-elastic media. Emphasis has been placed on introducing chemical effects into the coupled equation system. The procedure was fully coupled for both constitutive and governing equations, in the numerical results only the cases of chemical loads have been considered. The thermal contact problem of a piezoelectric strip with heat supply, generated by the frictional tangential traction under the action of a rigid sliding punch, has been investigated in [21]. The inertial effects were considered and numerical results were also presented. The solutions had a reduced dependence on the material properties.

In the last decades, several works have discussed the multifield analysis of multilayered plates, they have given different solution methodologies and interesting results with some limitations. These works concern exact and three-dimensional solutions, analytical, numerical and finite element methods. In this part of the introduction we discuss the main aspects of these works to point out the main innovations of the present article. Dube et al. [22] have proposed an exact piezothermoelastic solution for infinitely long, simply-supported, orthotropic, piezoelectric, flat panel in cylindrical bending under pressure, thermal and electrostatic excitation. The governing equations have been reduced to ordinary differential equations with constant coefficients. In the linear constitutive equations, the thermal field was partially coupled, in fact, the Fourier heat conduction equation has been added to the equations of equilibrium for stresses and electric displacements.

Other interesting exact solutions for static analysis of thermoelectroelastic laminated plates have been given in [23]. In this work, a new concise procedure for the analytical solution of composite laminated plates with piezoelectric layers has been developed. Numerical studies have been conducted on a five-layer piezoelectric plate and the complexity of stresses and deformations under combined loading has been illustrated, however the temperature was only considered as external load. A similar solution has been proposed in [24] where composite laminates with piezo-thermo-elastic layers under cylindrical bending have been investigated. The analytical examples have demonstrated the complexity of both the stress distribution and the deformation response when combined loading conditions were considered,

results were not fully coupled in terms of thermal field. Kapuria and Nair [25] have proposed an exact three-dimensional piezothermoelasticity solution for static, free vibration and steady-state harmonic response of simply supported cross-ply piezoelectric (hybrid) laminated rectangular plates with interlaminar bonding imperfections. Numerical results were presented for hybrid composite and sandwich plates with varying imperfection compliance. The solution was not fully coupled in terms of temperature field but three loading cases have been presented: applied pressure, imposed electric potential and imposed temperature. A fully coupling in constitutive equations, gradient equations and equilibrium equations has been proposed in [26] where Xu et al. have given analytic three-dimensional solutions for the coupled thermoelectroelastic response of multilayered hybrid composite plates. An analytical higher order zig-zag plate theory has been developed in [27] to refine the prediction of the mechanical, thermal, and electric behaviors of composite plates embedding piezoelectric layers.

In-plane displacements were cubic expanded, the transverse displacement was quadratic expanded, a Heaviside unit step function was added to in-plane displacements to recover the zig-zag effect. Krommer [28] has investigated thermally induced vibrations of laminated plates with attached or embedded piezoelectric layers. The modeling was based on the kinematic assumption of Kirchhoff; consistently, the thickness distribution of the electric potential was considered being of second order. The plate theory has incorporated the direct piezoelectric effect by means of effective plate stiffness, and the pyroelectric effect by means of effective thermal loading. Further higher-order zig-zag theories have been proposed in [29] to accurately calculate the static response of smart plates subjected to mechanical, thermal and electric loads.

All variables were in zig-zag form: cubic in-plane displacements and quadratic transverse displacements, cubic temperature and linear electric potential. In the Vel dissertation [30] the Eshelby-Stroh formalism was used to analyze the generalized plane strain quasi-static deformation of an anisotropic, linear elastic laminated plate. This formalism was extended to study the generalized plane deformations of piezothermoelastic laminated plates. The method was capable of analyzing laminated plates with embedded piezothermoleastic patches. The theory of piezoelasticity has been extended to a functionally graded piezoelectric sandwich cantilever under an applied electric field and/or a heat load in [31].

The temperature in the constitutive equations was not fully coupled, Fourier heat conduction equation was added to equilibrium equations for stresses and electric displacements. Static and dynamic electro-thermo-mechanical analysis of angle-ply hybrid piezoelectric beams using a recently developed efficient coupled zig-zag theory has been presented in [32]. Liew et al. [33] have investigated the behaviour of multilayered composite plates subject to thermo-piezoelectric-mechanical loadings. The analysis was performed using the three-dimensional equations of thermo-piezoelasticity and the differential quadrature (DQ) numerical technique. The equilibrium equations were written for stresses (3D indefinite equilibrium equations), electric displacements (in analogy with stresses) and temperature (Fourier heat conduction equation). No full coupling was considered in [34] where the nonlinear bending analysis of a simply supported laminated plate with piezoelectric actuators subjected to a transverse uniform or sinusoidal electrical and thermal loads was given.

A large amplitude vibration analysis of pre-stressed functionally graded material (FGM) laminated plates embedding two surface-mounted piezoelectric actuator layers has been given in [35], nonlinear governing equations of motion were derived within the context of Reddy higher-order shear deformation plate theory. Yang and Xiang [36] have investigated the static bending, free vibration, and dynamic response of monomorph, bimorph, and multimorph actuators made of functionally graded piezoelectric materials under a combined thermal-electro-mechanical load by using the Timoshenko beam theory. The partially coupled governing differential equations were solved using the differential quadrature method. Several interesting Finite Element (FE) results can be found in [37] where three-dimensional FE elements by MSC/NASTRAN have been used in order to discuss the analogy between piezoelectric and thermal fields to obtain results for different loading conditions applied to piezoceramic and aluminium cantilever beams.

Giannopoulos and Vantomme [38] have presented the dynamic analysis of composite plates incorporating piezoelectric layers, a 4-node plate finite element incorporating discrete layer kinematic assumptions has been used to assess the dynamic performance of a smart plate under different thermal, mechanical and electrical conditions. In [39] the results of the coupled theory have been compared with those obtained using the conventional uncoupled theory, in the FE analysis of composite plates a higher-order temperature field theory was developed to accurately model the temperature distribution in laminated structures. Mechanical, electrical and thermal response of piezoelectric composite laminates and plate structures has been investigated in [40]. A layer-wise theory was developed to model the active and sensory response of such structures in thermal environments.

Finite element equations were derived for a bi-linear 4-noded plate element. In-plane displacements, electric potential and temperature were considered in LW form, as the transverse displacement was constant. The governing equations were not fully coupled because the temperature was considered as an external load. A fully-coupling for both constitutive and governing equations has been proposed in [41], where all variables were in zigzag form and a three-node triangular finite element was developed. The response of composite plates constructed of graphite/epoxy laminae with an attached piezoelectric polyvinylidene fluoride layer subjected to mechanical, thermal and electric field loading has been considered in [42]. First-order shear deformation theory was extended to include the piezothermoelastic response of composite plate structures; electrical and thermal fields were seen as external loads.

The present work gives refined two-dimensional models that allow to obtain fully coupled thermo-electro-mechanical governing equations for the static investigation of multilayered plates. Such governing equations enable to analyze the limitations of classical theories and the multifield effects. Next the fully coupled thermopiezoelectric constitutive equations are derived, a unified formulation is then described, which allows to obtain several layer wise and equivalent single layer refined two dimensional models for plates. Multi-field geometrical relations for plates are detailed in and the Principle of Virtual Displacements is proposed to be extended to the thermo-electro-mechanical cases to obtain fully coupled governing equations with displacements, electric potential and temperature as primary variables. Such governing equations are solved in a closed form; and, the

acronyms for the different refined models obtained are discussed. Finally, results are proposed (both assessments with the open literature and new benchmarks) and conclusions are pointed out.

CONSTITUTIVE EQUATIONS

Materials and their reactions to applied multifield loads are characterized by constitutive equations. Their thermo-electro-mechanical form is obtained in this section according to that reported in [1] and [2]. The general coupling between the mechanical, electrical and thermal fields is determined here using thermodynamical principles and Maxwell relations [7, 8]. First, it is necessary to define a *Gibbs free-energy function G* and then, a *thermopiezoelectric enthalpy density H* [4, 9]:

$$G(\epsilon_{ij}, \mathscr{E}_i, \theta) = \sigma_{ij}\epsilon_{ij} - \mathscr{E}_i\mathscr{D}_i - \eta\theta, \tag{1}$$

$$H(\epsilon_{ij}, \mathscr{E}_i, \theta, \vartheta_i) = G(\epsilon_{ij}, \mathscr{E}_i, \theta) - F(\vartheta_i), \tag{2}$$

where σ_{ij} and ϵ_{ij} are the stress and strain components, $\mathscr{E}_i$ is the electric field vector, and $\mathscr{D}_i$ is the electric displacement vector. η is the variation in entropy per unit of volume and θ the temperature considered with respect to the reference temperature T_0. The function $F(\vartheta_i)$ is called a dissipation function, and it depends on the spatial temperature gradient ϑ_i:

$$F(\vartheta_i) = \frac{1}{2}\kappa_{ij}\vartheta_i\vartheta_j - \tau_0\dot{h}_i, \tag{3}$$

where κ_{ij} is the symmetric, positive, semidefinite conductivity tensor. In the second term, τ_0 is a thermal relaxation parameter and $\dot{h}_i$ is the temporal derivative of the heat flux h_i. The thermal relaxation parameter is usually omitted in such multifield problems. Further details about the dissipation function $F(\vartheta_i)$ are given in [7, 8] and [9], where interesting considerations are made about the inclusion or lack of inclusion of the dissipation function $F(\vartheta_i)$.

In the case of a linear interaction, the thermopiezoelectric enthalpy density H can be expanded in a quadratic form:

$$\begin{aligned} H(\epsilon_{ij}, \mathscr{E}_i, \theta, \vartheta_i) = {} & \frac{1}{2}Q_{ijkl}\epsilon_{ij}\epsilon_{kl} - e_{ijk}\epsilon_{ij}\mathscr{E}_k - \lambda_{ij}\epsilon_{ij}\theta - \frac{1}{2}\varepsilon_{kl}\mathscr{E}_k\mathscr{E}_l - p_k\mathscr{E}_k\theta \\ & - \frac{1}{2}\chi\theta^2 - \frac{1}{2}\kappa_{ij}\vartheta_i\vartheta_j, \end{aligned} \tag{4}$$

where Q_{ijkl} is the elastic coefficients tensor considered for an orthotropic material in the problem reference system [2]. e_{ijk} are the piezoelectric coefficients and ε_{kl} are the permittivity coefficients [6]. λ_{ij} are thermo-mechanical coupling coefficients and p_k are the pyroelectric coefficients. $\chi = \frac{\rho C_v}{T_0}$ where ρ is the material density, C_v is the specific heat per unit mass and T_0 is the reference temperature [3].

The constitutive equations are obtained via partial derivatives:

$$\sigma_{ij} = \frac{\partial H}{\partial \epsilon_{ij}}, \quad \mathscr{D}_k = -\frac{\partial H}{\partial \mathscr{E}_k}, \quad \eta = -\frac{\partial H}{\partial \theta}, \quad h_i = -\frac{\partial H}{\partial \vartheta_i}. \tag{5}$$

The constitutive equations for the thermo-electro-mechanical problem are obtained from Eqs. (4) and (5):

$$\sigma_{ij} = Q_{ijkl}\epsilon_{kl} - e_{ijk}\mathscr{E}_k - \lambda_{ij}\theta, \tag{6}$$

$$\mathscr{D}_k = e_{ijk}\epsilon_{ij} + \varepsilon_{kl}\mathscr{E}_l + p_k\theta, \tag{7}$$

$$\eta = \lambda_{ij}\epsilon_{ij} + p_k\mathscr{E}_k + \chi\theta, \tag{8}$$

$$h_i = \kappa_{ij}\vartheta_j. \tag{9}$$

These equations can be written in single-subscript notation by using the indexes $m = q = 1, 2, 3, 4, 5, 6$ and $i = j = 1, 2, 3$:

$$\sigma_m = Q_{mq}\epsilon_q - e_{mi}\mathscr{E}_i - \lambda_m\theta, \tag{10}$$

$$\mathscr{D}_i = e_{iq}\epsilon_q + \varepsilon_{ij}\mathscr{E}_j + p_i\theta, \tag{11}$$

$$\eta = \lambda_q\epsilon_q + p_j\mathscr{E}_j + \chi\theta, \tag{12}$$

$$h_i = \kappa_{ij}\vartheta_j. \tag{13}$$

The matrix form is obtained from the equations written in single-subscript notations; the matrices and vectors are indicated in bold scripture. Considering a generic multilayered structure, Eqs. (10)–(13) are written for a generic k layer in the problem reference system (x, y, z) as:

$$\boldsymbol{\sigma}^k = \boldsymbol{Q}^k\boldsymbol{\epsilon}^k - \boldsymbol{e}^{kT}\boldsymbol{\mathscr{E}}^k - \boldsymbol{\lambda}^k\theta^k, \tag{14}$$

$$\boldsymbol{\mathscr{D}}^k = \boldsymbol{e}^k\boldsymbol{\epsilon}^k + \boldsymbol{\varepsilon}^k\boldsymbol{\mathscr{E}}^k + \boldsymbol{p}^k\theta^k, \tag{15}$$

$$\eta^k = \boldsymbol{\lambda}^{kT}\boldsymbol{\epsilon}^k + \boldsymbol{p}^{kT}\boldsymbol{\mathscr{E}}^k + \chi^k\theta^k, \tag{16}$$

$$\boldsymbol{h}^k = \boldsymbol{\kappa}^k\boldsymbol{\vartheta}^k, \tag{17}$$

where the sovra-temperature θ^k (temperature T_1 referred to reference temperature T_0, $\theta = T_1 - T_0$), the term χ^k and the entropy per unit volume η^k are scalar variables in each k layer. The 6×1 vectors of stress and strain components are:

$$\boldsymbol{\sigma}^k = \begin{Bmatrix} \sigma_{xx} \\ \sigma_{yy} \\ \sigma_{zz} \\ \sigma_{yz} \\ \sigma_{xz} \\ \sigma_{xy} \end{Bmatrix}^k, \quad \boldsymbol{\epsilon}^k = \begin{Bmatrix} \epsilon_{xx} \\ \epsilon_{yy} \\ \epsilon_{zz} \\ \gamma_{yz} \\ \gamma_{xz} \\ \gamma_{xy} \end{Bmatrix}^k. \tag{18}$$

The 3×1 vectors of electrical field $\boldsymbol{\mathscr{E}}^k$, electrical displacement $\boldsymbol{\mathscr{D}}^k$, heat flux $\boldsymbol{h}^k$ and spatial gradient of temperature $\boldsymbol{\vartheta}^k$ are:

$$\boldsymbol{\mathscr{E}}^k = \begin{Bmatrix} \mathscr{E}_x \\ \mathscr{E}_y \\ \mathscr{E}_z \end{Bmatrix}^k, \quad \boldsymbol{\mathscr{D}}^k = \begin{Bmatrix} \mathscr{D}_x \\ \mathscr{D}_y \\ \mathscr{D}_z \end{Bmatrix}^k, \quad \boldsymbol{h}^k = \begin{Bmatrix} h_x \\ h_y \\ h_z \end{Bmatrix}^k, \quad \boldsymbol{\vartheta}^k = \begin{Bmatrix} \vartheta_x \\ \vartheta_y \\ \vartheta_z \end{Bmatrix}^k. \tag{19}$$

The 3×1 array of pyroelectric coefficients $\boldsymbol{p}^k$ and the 6×1 array of thermo-mechanical coupling coefficients $\boldsymbol{\lambda}^k$ are:

$$\boldsymbol{p}^k = \begin{Bmatrix} p_1 \\ p_2 \\ p_3 \end{Bmatrix}^k, \quad \boldsymbol{\lambda}^k = \boldsymbol{Q}^k \, \boldsymbol{\alpha}^k = \begin{Bmatrix} \lambda_1 \\ \lambda_2 \\ \lambda_3 \\ 0 \\ 0 \\ \lambda_6 \end{Bmatrix}^k, \tag{20}$$

where the elastic coefficients matrix $\boldsymbol{Q}^k$ of Hooke's law in problem reference system for an orthotropic material is:

$$\boldsymbol{Q}^k = \begin{bmatrix} Q_{11} & Q_{12} & Q_{13} & 0 & 0 & Q_{16} \\ Q_{12} & Q_{22} & Q_{23} & 0 & 0 & Q_{26} \\ Q_{13} & Q_{23} & Q_{33} & 0 & 0 & Q_{36} \\ 0 & 0 & 0 & Q_{44} & Q_{45} & 0 \\ 0 & 0 & 0 & Q_{45} & Q_{55} & 0 \\ Q_{16} & Q_{26} & Q_{36} & 0 & 0 & Q_{66} \end{bmatrix}^k, \tag{21}$$

the vector $\boldsymbol{\alpha}^k$ has dimension 6×1 and it contains the thermal expansion coefficients:

$$\boldsymbol{\alpha}^k = \begin{Bmatrix} \alpha_1 \\ \alpha_2 \\ \alpha_3 \\ 0 \\ 0 \\ 0 \end{Bmatrix}^k. \tag{22}$$

The matrices $\boldsymbol{\varepsilon}^k$ of permittivity coefficients and $\boldsymbol{\kappa}^k$ of conductivity coefficients have dimension 3×3:

$$\boldsymbol{\varepsilon}^k = \begin{bmatrix} \varepsilon_{11} & \varepsilon_{12} & 0 \\ \varepsilon_{12} & \varepsilon_{22} & 0 \\ 0 & 0 & \varepsilon_{33} \end{bmatrix}^k, \quad \boldsymbol{\kappa}^k = \begin{bmatrix} \kappa_{11} & \kappa_{12} & 0 \\ \kappa_{12} & \kappa_{22} & 0 \\ 0 & 0 & \kappa_{33} \end{bmatrix}^k. \tag{23}$$

The matrix of piezoelectric coefficients $\boldsymbol{e}^k$ has dimension 3×6:

$$\boldsymbol{e}^k = \begin{bmatrix} 0 & 0 & 0 & e_{14} & e_{15} & 0 \\ 0 & 0 & 0 & e_{24} & e_{25} & 0 \\ e_{31} & e_{32} & e_{33} & 0 & 0 & e_{36} \end{bmatrix}^k. \tag{24}$$

The relations proposed in Eqs. (14)–(17) will be introduced in the variational statements (which will be presented later) after their split into in-plane components

(subscript p) and out-of-plane components (subscript n). Two new subscripts are introduced: the subscript C for those variables in the variational statements that need the substitution of constitutive equations; the subscript G for those variables in constitutive equations that need the substitution of geometrical relations (these last will be introduced later). The split stress and strain component vectors are:

$$\boldsymbol{\sigma}_{pC}^k = \left\{ \begin{matrix} \sigma_{xx} \\ \sigma_{yy} \\ \sigma_{xy} \end{matrix} \right\}^k, \quad \boldsymbol{\sigma}_{nC}^k = \left\{ \begin{matrix} \sigma_{xz} \\ \sigma_{yz} \\ \sigma_{zz} \end{matrix} \right\}^k, \quad \boldsymbol{\epsilon}_{pG}^k = \left\{ \begin{matrix} \epsilon_{xx} \\ \epsilon_{yy} \\ \gamma_{xy} \end{matrix} \right\}^k, \quad \boldsymbol{\epsilon}_{nG}^k = \left\{ \begin{matrix} \gamma_{xz} \\ \gamma_{yz} \\ \epsilon_{zz} \end{matrix} \right\}^k. \tag{25}$$

The 3×1 vectors of electrical displacement, electrical field, heat flux and spatial gradient of the temperature are split into in-plane and out-plane components:

$$\mathscr{D}_{pC}^k = \left\{ \begin{matrix} \mathscr{D}_x \\ \mathscr{D}_y \end{matrix} \right\}^k, \quad \mathscr{D}_{nC}^k = \left\{ \mathscr{D}_z \right\}^k, \quad \mathscr{E}_{pG}^k = \left\{ \begin{matrix} \mathscr{E}_x \\ \mathscr{E}_y \end{matrix} \right\}^k, \quad \mathscr{E}_{nG}^k = \left\{ \mathscr{E}_z \right\}^k, \tag{26}$$

$$\boldsymbol{h}_{pC}^k = \left\{ \begin{matrix} h_x \\ h_y \end{matrix} \right\}^k, \quad \boldsymbol{h}_{nC}^k = \left\{ h_z \right\}^k, \quad \boldsymbol{\vartheta}_{pG}^k = \left\{ \begin{matrix} \vartheta_x \\ \vartheta_y \end{matrix} \right\}^k, \quad \boldsymbol{\vartheta}_{nG}^k = \left\{ \vartheta_z \right\}^k.$$

Therefore, the split form of Eqs. (14)–(17) is:

$$\boldsymbol{\sigma}_{pC}^k = \boldsymbol{Q}_{pp}^k \boldsymbol{\epsilon}_{pG}^k + \boldsymbol{Q}_{pn}^k \boldsymbol{\epsilon}_{nG}^k - \boldsymbol{e}_{pp}^{kT} \mathscr{E}_{pG}^k - \boldsymbol{e}_{np}^{kT} \mathscr{E}_{nG}^k - \boldsymbol{\lambda}_p^k \theta^k, \tag{27}$$

$$\boldsymbol{\sigma}_{nC}^k = \boldsymbol{Q}_{np}^k \boldsymbol{\epsilon}_{pG}^k + \boldsymbol{Q}_{nn}^k \boldsymbol{\epsilon}_{nG}^k - \boldsymbol{e}_{pn}^{kT} \mathscr{E}_{pG}^k - \boldsymbol{e}_{nn}^{kT} \mathscr{E}_{nG}^k - \boldsymbol{\lambda}_n^k \theta^k, \tag{28}$$

$$\mathscr{D}_{pC}^k = \boldsymbol{e}_{pp}^k \boldsymbol{\epsilon}_{pG}^k + \boldsymbol{e}_{pn}^k \boldsymbol{\epsilon}_{nG}^k + \boldsymbol{\varepsilon}_{pp}^k \mathscr{E}_{pG}^k + \boldsymbol{\varepsilon}_{pn}^k \mathscr{E}_{nG}^k + \boldsymbol{p}_p^k \theta^k, \tag{29}$$

$$\mathscr{D}_{nC}^k = \boldsymbol{e}_{np}^k \boldsymbol{\epsilon}_{pG}^k + \boldsymbol{e}_{nn}^k \boldsymbol{\epsilon}_{nG}^k + \boldsymbol{\varepsilon}_{np}^k \mathscr{E}_{pG}^k + \boldsymbol{\varepsilon}_{nn}^k \mathscr{E}_{nG}^k + \boldsymbol{p}_n^k \theta^k, \tag{30}$$

$$\eta_C^k = \boldsymbol{\lambda}_p^{kT} \boldsymbol{\epsilon}_{pG}^k + \boldsymbol{\lambda}_n^{kT} \boldsymbol{\epsilon}_{nG}^k + \boldsymbol{p}_p^{kT} \mathscr{E}_{pG}^k + \boldsymbol{p}_n^{kT} \mathscr{E}_{nG}^k + \chi^k \theta^k, \tag{31}$$

$$\boldsymbol{h}_p^k = \boldsymbol{\kappa}_{pp}^k \boldsymbol{\vartheta}_{pG}^k + \boldsymbol{\kappa}_{pn}^k \boldsymbol{\vartheta}_{nG}^k, \tag{32}$$

$$\boldsymbol{h}_n^k = \boldsymbol{\kappa}_{np}^k \boldsymbol{\vartheta}_{pG}^k + \boldsymbol{\kappa}_{nn}^k \boldsymbol{\vartheta}_{nG}^k. \tag{33}$$

The explicit forms of the new matrices in Eqs. (27)–(33) are given in the following arrays.

Elastic coefficient matrices are:

$$\boldsymbol{Q}_{pp}^k = \begin{bmatrix} Q_{11} & Q_{12} & Q_{16} \\ Q_{12} & Q_{22} & Q_{26} \\ Q_{16} & Q_{26} & Q_{66} \end{bmatrix}^k, \quad \boldsymbol{Q}_{pn}^k = \begin{bmatrix} 0 & 0 & Q_{13} \\ 0 & 0 & Q_{23} \\ 0 & 0 & Q_{36} \end{bmatrix}^k, \tag{34}$$

$$\boldsymbol{Q}_{np}^k = \begin{bmatrix} 0 & 0 & 0 \\ 0 & 0 & 0 \\ Q_{13} & Q_{23} & Q_{36} \end{bmatrix}^k, \quad \boldsymbol{Q}_{nn}^k = \begin{bmatrix} Q_{55} & Q_{45} & 0 \\ Q_{45} & Q_{44} & 0 \\ 0 & 0 & Q_{33} \end{bmatrix}^k.$$

Piezoelectric coefficients in split form are:

$$\boldsymbol{e}_{pp}^{k} = \begin{bmatrix} 0 & 0 & 0 \\ 0 & 0 & 0 \end{bmatrix}^{k}, \quad \boldsymbol{e}_{pn}^{k} = \begin{bmatrix} e_{15} & e_{14} & 0 \\ e_{25} & e_{24} & 0 \end{bmatrix}^{k}, \tag{35}$$

$$\boldsymbol{e}_{np}^{k} = \begin{bmatrix} e_{31} & e_{32} & e_{36} \end{bmatrix}^{k}, \quad \boldsymbol{e}_{nn}^{k} = \begin{bmatrix} 0 & 0 & e_{33} \end{bmatrix}^{k}.$$

Permittivity coefficients are split as:

$$\boldsymbol{\varepsilon}_{pp}^{k} = \begin{bmatrix} \varepsilon_{11} & \varepsilon_{12} \\ \varepsilon_{12} & \varepsilon_{22} \end{bmatrix}^{k}, \quad \boldsymbol{\varepsilon}_{pn}^{k} = \begin{bmatrix} 0 \\ 0 \end{bmatrix}^{k}, \tag{36}$$

$$\boldsymbol{\varepsilon}_{np}^{k} = \begin{bmatrix} 0 & 0 \end{bmatrix}^{k}, \quad \boldsymbol{\varepsilon}_{nn}^{k} = \begin{bmatrix} \varepsilon_{33} \end{bmatrix}^{k}.$$

Split forms of thermo-mechanical coupling coefficients are:

$$\boldsymbol{\lambda}_{p}^{k} = \begin{bmatrix} \lambda_1 \\ \lambda_2 \\ \lambda_6 \end{bmatrix}^{k}, \quad \boldsymbol{\lambda}_{n}^{k} = \begin{bmatrix} 0 \\ 0 \\ \lambda_3 \end{bmatrix}^{k}. \tag{37}$$

In-plane and out-of-plane pyroelectric coefficients are:

$$\boldsymbol{p}_{p}^{k} = \begin{bmatrix} p_1 \\ p_2 \end{bmatrix}^{k}, \quad \boldsymbol{p}_{n}^{k} = \begin{bmatrix} p_3 \end{bmatrix}^{k}. \tag{38}$$

Conductivity coefficients are given as four sub-matrices:

$$\boldsymbol{\kappa}_{pp}^{k} = \begin{bmatrix} \kappa_{11} & \kappa_{12} \\ \kappa_{12} & \kappa_{22} \end{bmatrix}^{k}, \quad \boldsymbol{\kappa}_{pn}^{k} = \begin{bmatrix} 0 \\ 0 \end{bmatrix}^{k}, \tag{39}$$
$$\boldsymbol{\kappa}_{np}^{k} = \begin{bmatrix} 0 & 0 \end{bmatrix}^{k}, \quad \boldsymbol{\kappa}_{nn}^{k} = \begin{bmatrix} \kappa_{33} \end{bmatrix}^{k}.$$

CARRERA UNIFIED FORMULATION (CUF)

Carrera Unified Formulation (CUF) gives, in a unified manner, a large variety of refined two-dimensional models [1, 2] for multifield analysis of multilayered structures. The governing equations are written in terms of a few fundamental nuclei that do not formally depend on the order of expansion N used in the thickness direction and on the description of variables (equivalent single layer (ESL) when the variable is assumed for the whole multilayer or layer-wise (LW) when the variable is considered independent in each layer). The application of a two-dimensional plate theory allows the unknown variables to be expressed as a set of thickness functions that only depend on the thickness coordinate z and the correspondent variable, which depends on the in-plane coordinates x and y. A generic variable $\boldsymbol{f}(x, y, z)$,

for example a displacement, and its variation $\delta \boldsymbol{f}(x, y, z)$ are written according to the following general expansion:

$$\boldsymbol{f}(x, y, z) = F_\tau(z)\boldsymbol{f}_\tau(x, y), \quad \delta \boldsymbol{f}(x, y, z) = F_s(z)\delta \boldsymbol{f}_s(x, y), \quad \textit{with} \quad \tau, s = 1, \ldots, N, \tag{40}$$

where the bold letters denote arrays, (x,y) are the in-plane coordinates and z the thickness one. The summing convention, with repeated indexes τ and s, is assumed. The order of expansion N goes from first to fourth-order. In the thermo-electro-mechanical models, displacements can be modelled in both ESL or LW form, sovra-temperature and electric potential are always considered in LW form. Therefore, a two-dimensional thermo-electro-mechanical plate model is defined as ESL or LW, depending on the choice made for the displacement vector.

Equivalent Single Layer (ESL) Approach

The displacement $\boldsymbol{u} = (u, v, w)$ is described in equivalent single layer (ESL) form if the unknowns are the same for the whole plate [2] (see the left part of Figure 1 where first and third-order expansions in a three-layered structure are given). The z Taylor expansion is:

$$\begin{aligned} u &= F_0 u_0 + F_1 u_1 + \cdots + F_N u_N = F_\tau u_\tau, \\ v &= F_0 v_0 + F_1 v_1 + \cdots + F_N v_N = F_\tau v_\tau, \\ w &= F_0 w_0 + F_1 w_1 + \cdots + F_N w_N = F_\tau\ w_\tau, \end{aligned} \tag{41}$$

with $\tau = 0, 1, \ldots, N$; N is the order of expansion that ranges from 1 (linear) to 4:

$$F_0 = z^0 = 1, \quad F_1 = z^1 = z, \quad \ldots, \quad F_N = z^N. \tag{42}$$

The vectorial form of Eq. (41) is:

$$\boldsymbol{u}(x, y, z) = F_\tau(z)\boldsymbol{u}_\tau(x, y), \quad \delta \boldsymbol{u}(x, y, z) = F_s(z)\delta \boldsymbol{u}_s(x, y), \quad \textit{with} \quad \tau, s = 1, \ldots, N. \tag{43}$$

Classical theories, such those which discard the ϵ_{zz} effect, can be obtained from refined ESL models. First-order Shear Deformation Theory (FSDT) [11, 12] is obtained from an ESL model with linear expansion in the thickness direction z, by

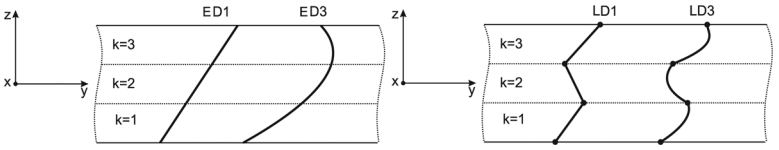

Figure 1 Equivalent Single Layer (ESL) vs. Layer Wise (LW) theories for the thermo-electro-mechanical variables of a multilayered smart plate.

imposing a constant transverse displacement w in z. Classical Lamination Theory (CLT) [10] is obtained from FSDT via an opportune penalty technique which imposes an infinite transverse shear rigidity.

Layer-Wise (LW) approach

In a layer-wise (LW) approach, each layer of a multilayered structure is described as independent plates [2]. The displacement $\boldsymbol{u}^k = (u, v, w)^k$ is modelled for each layer k, in this way the zigzag form of displacement is easily obtained (see the right part of Figure 1 for the example of first and third order expansions through the thickness direction of a three layered structure). The z expansion for displacement components is made for each layer k:

$$\begin{aligned} u^k &= F_0 u_0^k + F_1 u_1^k + \cdots + F_N u_N^k = F_\tau u_\tau^k, \\ v^k &= F_0 v_0^k + F_1 v_1^k + \cdots + F_N v_N^k = F_\tau v_\tau^k, \\ w^k &= F_0 w_0^k + F_1 w_1^k + \cdots + F_N w_N^k = F_\tau w_\tau^k, \end{aligned} \tag{44}$$

with $\tau = 0, 1, \ldots, N$, N is the order of expansion that ranges from 1 (linear) to 4. $k = 1, \ldots, N_l$, where N_l indicates the number of layers. Eq. (44) written in a vectorial form is:

$$\begin{aligned} &\boldsymbol{u}^k(x, y, z) = F_\tau(z)\boldsymbol{u}_\tau^k(x, y), \quad \delta\boldsymbol{u}^k(x, y, z) = F_s(z)\delta\boldsymbol{u}_s^k(x, y), \\ &\quad \text{with } \tau, s = t, b, r \text{ and } k = 1, \ldots, N_l, \end{aligned} \tag{45}$$

where t and b indicate the top and bottom of each k layer, respectively; r indicates the higher orders of expansion in the thickness direction: $r = 2, \ldots, N$. The thickness functions $F_\tau(\zeta_k)$ and $F_s(\zeta_k)$ have been defined at the k-layer level, they are a linear combination of Legendre polynomials $P_j = P_j(\zeta_k)$ of the j^{th}-order defined in ζ_k-domain ($\zeta_k = \frac{2z_k}{h_k}$ where z_k is the local coordinate and h_k is the thickness, both quantities are referred to k^{th} layer, so $-1 \leq \zeta_k \leq 1$). The first five Legendre polynomials are:

$$\begin{aligned} &P_0 = 1, \quad P_1 = \zeta_k, \quad P_2 = \frac{(3{\zeta_k}^2 - 1)}{2}, \quad P_3 = \frac{5{\zeta_k}^3}{2} - \frac{3\zeta_k}{2}, \\ &P_4 = \frac{35{\zeta_k}^4}{8} - \frac{15{\zeta_k}^2}{4} + \frac{3}{8}, \end{aligned} \tag{46}$$

their combinations for the thickness functions are:

$$F_t = F_0 = \frac{P_0 + P_1}{2}, \quad F_b = F_1 = \frac{P_0 - P_1}{2}, \quad F_r = P_r - P_{r-2} \quad with \quad r = 2, \ldots, N. \tag{47}$$

The following interesting properties of the chosen functions allow to consider interface values of the variables as variable unknowns, see Figure 1. This feature

easily allows the compatibility conditions for displacements at each layer interface to be imposed:

$$\zeta_k = 1 \quad : F_t = 1; \quad F_b = 0; \quad F_r = 0 \quad \textit{at top}, \tag{48}$$

$$\zeta_k = -1 \quad : F_t = 0; \quad F_b = 1; \quad F_r = 0 \quad \textit{at bottom}. \tag{49}$$

In case of thermo-electro-mechanical problems, the primary variables are the displacement vector $\boldsymbol{u} = (u, v, w)$, the electric potential Φ and the scalar sovra-temperature θ (temperature T_1 referred to the reference external room temperature T_0, $\theta = T_1 - T_0$). By considering the higher spatial gradient of the electric potential and temperature field, the variables Φ^k and θ^k are always modelled as LW [2, 3]:

$$\Phi^k(x, y, z) = F_\tau(z)\Phi^k_\tau(x, y), \quad \delta\Phi^k(x, y, z) = F_s(z)\delta\Phi^k_s(x, y), \tag{50}$$
$$\textit{with} \quad \tau, s = t, b, r \quad \textit{and} \quad k = 1, \ldots, N_l,$$

$$\theta^k(x, y, z) = F_\tau(z)\theta^k_\tau(x, y), \quad \delta\theta^k(x, y, z) = F_s(z)\delta\theta^k_s(x, y), \tag{51}$$
$$\textit{with} \quad \tau, s = t, b, r \quad \textit{and} \quad k = 1, \ldots, N_l,$$

The thickness functions are a combination of Legendre polynomials as indicated in Eqs. (46) and (47). This LW form also permits to easily impose the electric voltage or temperature value on the surfaces. A two-dimensional model for thermo-electro-mechanical problems is defined as ESL or LW, depending on the choice made for the displacement vector: the electric potential and temperature are always considered in LW form.

GEOMETRICAL RELATIONS

A thin plate is a three-dimensional body bounded by two closely spaced surfaces, the distance between the two surfaces must be small in comparison with the other dimensions. Its middle surface is the locus of points that lie midway between these surfaces. The distance between the surfaces measured along the normal to the middle surface is the thickness of the plate at that point [43]. The chosen reference system (x, y, z) is a rectilinear Cartesian one [44]. The in-plane dimensions are indicated with a and b in x and y directions, respectively. The thickness value in z direction is indicated with h, details are given in Figure 2. The thermo-electro-mechanical geometrical relations for plates link the mechanical strains with the displacement vector, the electric field with the scalar electric potential and the spatial gradient of temperature with the scalar sovra-temperature. The relations split in in-plane (p) and out-of-plane (n) components are:

$$\boldsymbol{\epsilon}^k_{pG} = [\epsilon_{xx}, \epsilon_{yy}, \gamma_{xy}]^{kT} = \boldsymbol{D}_p\boldsymbol{u}^k, \tag{52}$$

$$\boldsymbol{\epsilon}^k_{nG} = [\gamma_{xz}, \gamma_{yz}, \epsilon_{zz}]^{kT} = (\boldsymbol{D}_{np} + \boldsymbol{D}_{nz})\boldsymbol{u}^k, \tag{53}$$

$$\boldsymbol{\mathscr{E}}^k_{pG} = [\mathscr{E}_x, \mathscr{E}_y]^{kT} = -\boldsymbol{D}_{ep}\Phi^k, \tag{54}$$

$$\boldsymbol{\mathscr{E}}^k_{nG} = [\mathscr{E}_z]^k = -\boldsymbol{D}_{en}\Phi^k, \tag{55}$$

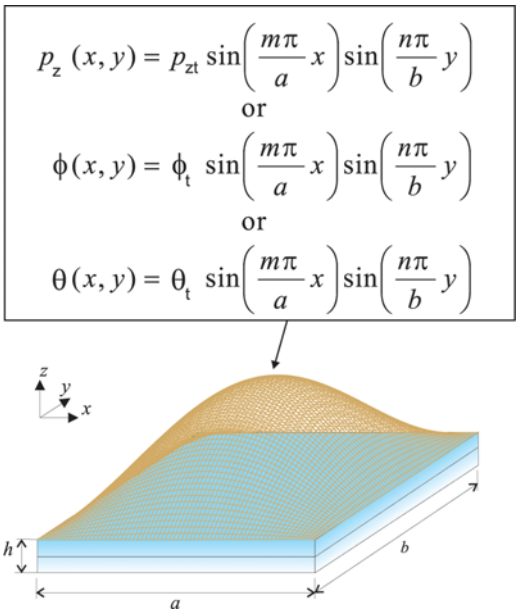

Figure 2 Geometry and load configurations for a multilayered smart plate. (color figure available online.)

$$\boldsymbol{\vartheta}_{pG}^{k} = [\vartheta_x, \vartheta_y]^{kT} = -\boldsymbol{D}_{tp}\theta^k, \tag{56}$$

$$\boldsymbol{\vartheta}_{nG}^{k} = [\vartheta_z]^{k} = -\boldsymbol{D}_{tn}\theta^k. \tag{57}$$

$\boldsymbol{\epsilon}_{pG}^{k}$ and $\boldsymbol{\epsilon}_{nG}^{k}$ are the in-plane and transverse strains, respectively. $\boldsymbol{u}^k = (u, v, w)^k$ is the displacement vector. $\boldsymbol{\mathcal{E}}_{pG}^{k}$ and $\boldsymbol{\mathcal{E}}_{nG}^{k}$ are in-plane and transverse electric field components, respectively. Φ^k is the scalar electric potential. $\boldsymbol{\vartheta}_{pG}^{k}$ and $\boldsymbol{\vartheta}_{nG}^{k}$ are in-plane and transverse spatial gradients of temperature, respectively. θ^k is the scalar temperature referred to the reference external room temperature. T means the transpose of a vector. The differential operators do not depend on the layer k in the case of a plate:

$$\boldsymbol{D}_p = \begin{bmatrix} \partial_x & 0 & 0 \\ 0 & \partial_y & 0 \\ \partial_y & \partial_x & 0 \end{bmatrix}, \quad \boldsymbol{D}_{np} = \begin{bmatrix} 0 & 0 & \partial_x \\ 0 & 0 & \partial_y \\ 0 & 0 & 0 \end{bmatrix}, \quad \boldsymbol{D}_{nz} = \begin{bmatrix} \partial_z & 0 & 0 \\ 0 & \partial_z & 0 \\ 0 & 0 & \partial_z \end{bmatrix}, \tag{58}$$

$$\boldsymbol{D}_{ep} = \boldsymbol{D}_{tp} = \begin{bmatrix} \partial_x \\ \partial_y \end{bmatrix}, \quad \boldsymbol{D}_{en} = \boldsymbol{D}_{tn} = \begin{bmatrix} \partial_z \end{bmatrix}.$$

The symbols in differential operators matrices indicate the partial derivatives: $\partial_x = \frac{\partial}{\partial x}$, $\partial_y = \frac{\partial}{\partial y}$ and $\partial_z = \frac{\partial}{\partial z}$.

PRINCIPLE OF VIRTUAL DISPLACEMENTS (PVD) EXTENDED TO MULTIFIELD ANALYSIS

In case of fully coupling between the mechanical, electrical and thermal fields, the variational statement is the PVD with the introduction of the virtual internal electrical and thermal works. This variational statement is:

$$\int_V \left(\delta\boldsymbol{\epsilon}_{pG}^T\boldsymbol{\sigma}_{pC} + \delta\boldsymbol{\epsilon}_{nG}^T\boldsymbol{\sigma}_{nC} - \delta\mathscr{E}_{pG}^T\mathscr{D}_{pC} - \delta\mathscr{E}_{nG}^T\mathscr{D}_{nC} - \delta\theta\eta_C - \delta\boldsymbol{\vartheta}_{pG}^T\boldsymbol{h}_{pC} - \delta\boldsymbol{\vartheta}_{nG}^T\boldsymbol{h}_{nC}\right)dV = \delta L_e - \delta L_{in}. \tag{59}$$

By considering a laminate of N_l layers and the volume V_k for each layer k as an integral on the in-plane surface Ω_k and an integral in the thickness direction domain A_k, the Eq. (59) can be rewritten as:

$$\sum_{k=1}^{N_l}\int_{\Omega_k}\int_{A_k}\left\{\delta\boldsymbol{\epsilon}_{pG}^{k\,T}\boldsymbol{\sigma}_{pC}^k + \delta\boldsymbol{\epsilon}_{nG}^{k\,T}\boldsymbol{\sigma}_{nC}^k - \delta\mathscr{E}_{pG}^{k\,T}\mathscr{D}_{pC}^k - \delta\mathscr{E}_{nG}^{k\,T}\mathscr{D}_{nC}^k - \delta\theta^k\eta_C^k - \delta\boldsymbol{\vartheta}_{pG}^{k\,T}\boldsymbol{h}_{pC}^k - \delta\boldsymbol{\vartheta}_{nG}^{k\,T}\boldsymbol{h}_{nC}^k\right\}d\Omega_k dz = \sum_{k=1}^{N_l}\delta L_e^k - \sum_{k=1}^{N_l}\delta L_{in}^k, \tag{60}$$

where δL_e^k and δL_{in}^k are the external and inertial virtual work at the k-layer level, respectively.

The governing equations have the following form:

$$\begin{aligned}
\delta\boldsymbol{u}_s^k &: \boldsymbol{K}_{uu}^{k\tau s}\boldsymbol{u}_\tau^k + \boldsymbol{K}_{u\Phi}^{k\tau s}\Phi_\tau^k + \boldsymbol{K}_{u\theta}^{k\tau s}\theta_\tau^k = \boldsymbol{p}_{us}^k - \boldsymbol{M}_{uu}^{k\tau s}\ddot{\boldsymbol{u}}_\tau^k \\
\delta\Phi_s^k &: \boldsymbol{K}_{\Phi u}^{k\tau s}\boldsymbol{u}_\tau^k + \boldsymbol{K}_{\Phi\Phi}^{k\tau s}\Phi_\tau^k + \boldsymbol{K}_{\Phi\theta}^{k\tau s}\theta_\tau^k = \boldsymbol{p}_{\Phi s}^k \\
\delta\theta_s^k &: \boldsymbol{K}_{\theta u}^{k\tau s}\boldsymbol{u}_\tau^k + \boldsymbol{K}_{\theta\Phi}^{k\tau s}\Phi_\tau^k + \boldsymbol{K}_{\theta\theta}^{k\tau s}\theta_\tau^k = \boldsymbol{p}_{\theta s}^k.
\end{aligned} \tag{61}$$

The arrays $\boldsymbol{p}_{us}^k$, $\boldsymbol{p}_{\Phi s}^k$ and $\boldsymbol{p}_{\theta s}^k$ indicate the variationally consistent mechanical, electrical and thermal loadings, respectively. Along with these governing equations the following boundary conditions on the edge Γ_k of the in-plane integration domain Ω_k hold:

$$\begin{aligned}
\boldsymbol{\Pi}_{uu}^{k\tau s}\boldsymbol{u}_\tau^k + \boldsymbol{\Pi}_{u\Phi}^{k\tau s}\Phi_\tau^k + \boldsymbol{\Pi}_{u\theta}^{k\tau s}\theta_\tau^k &= \boldsymbol{\Pi}_{uu}^{k\tau s}\bar{\boldsymbol{u}}_\tau^k + \boldsymbol{\Pi}_{u\Phi}^{k\tau s}\bar{\Phi}_\tau^k + \boldsymbol{\Pi}_{u\theta}^{k\tau s}\bar{\theta}_\tau^k \\
\boldsymbol{\Pi}_{\Phi u}^{k\tau s}\boldsymbol{u}_\tau^k + \boldsymbol{\Pi}_{\Phi\Phi}^{k\tau s}\Phi_\tau^k + \boldsymbol{\Pi}_{\Phi\theta}^{k\tau s}\theta_\tau^k &= \boldsymbol{\Pi}_{\Phi u}^{k\tau s}\bar{\boldsymbol{u}}_\tau^k + \boldsymbol{\Pi}_{\Phi\Phi}^{k\tau s}\bar{\Phi}_\tau^k + \boldsymbol{\Pi}_{\Phi\theta}^{k\tau s}\bar{\theta}_\tau^k \\
\boldsymbol{\Pi}_{\theta u}^{k\tau s}\boldsymbol{u}_\tau^k + \boldsymbol{\Pi}_{\theta\Phi}^{k\tau s}\Phi_\tau^k + \boldsymbol{\Pi}_{\theta\theta}^{k\tau s}\theta_\tau^k &= \boldsymbol{\Pi}_{\theta u}^{k\tau s}\bar{\boldsymbol{u}}_\tau^k + \boldsymbol{\Pi}_{\theta\Phi}^{k\tau s}\bar{\Phi}_\tau^k + \boldsymbol{\Pi}_{\theta\theta}^{k\tau s}\bar{\theta}_\tau^k.
\end{aligned} \tag{62}$$

The electric potential Φ^k and the sovra-temperature θ^k are variables of the problem. The displacements $\boldsymbol{u}^k$ can be seen in ESL or LW form. Independently by the choice made for the displacements, the electric potential and the sovra-temperature are always seen in LW form.

The variational statement includes only the internal thermal work made by the temperature in the case of mechanical load or imposed electric potential applied on the structure; it includes the internal thermal work made by the gradient of temperature in the case of temperature applied at the top and bottom of the structure.

PVD for Mechanical and Electrical Loads

In the case of mechanical load or electric potential applied on the structure, the terms $\delta \boldsymbol{\vartheta}_{pG}^{k\,T} \boldsymbol{h}_{pC}^{k}$ and $\delta \boldsymbol{\vartheta}_{nG}^{k\,T} \boldsymbol{h}_{nC}^{k}$ in the Eq. (60) are not considered because it does not exist a gradient of temperature. Therefore, the variational statement is:

$$\sum_{k=1}^{N_l} \int_{\Omega_k} \int_{A_k} \left\{ \delta \boldsymbol{\epsilon}_{pG}^{k\,T} \boldsymbol{\sigma}_{pC}^{k} + \delta \boldsymbol{\epsilon}_{nG}^{k\,T} \boldsymbol{\sigma}_{nC}^{k} - \delta \boldsymbol{\mathscr{E}}_{pG}^{k\,T} \boldsymbol{\mathscr{D}}_{pC}^{k} - \delta \boldsymbol{\mathscr{E}}_{nG}^{k\,T} \boldsymbol{\mathscr{D}}_{nC}^{k} - \delta\theta^{k} \eta_{C}^{k} \right\} d\Omega_k dz$$
$$= \sum_{k=1}^{N_l} \delta L_e^k - \sum_{k=1}^{N_l} \delta L_{in}^k. \tag{63}$$

The constitutive equations, as obtained in Eqs. (27)–(33), simply discard the heat fluxes $\boldsymbol{h}_{pC}^{k}$ and $\boldsymbol{h}_{nC}^{k}$:

$$\boldsymbol{\sigma}_{pC}^{k} = \boldsymbol{Q}_{pp}^{k} \boldsymbol{\epsilon}_{pG}^{k} + \boldsymbol{Q}_{pn}^{k} \boldsymbol{\epsilon}_{nG}^{k} - \boldsymbol{e}_{pp}^{kT} \boldsymbol{\mathscr{E}}_{pG}^{k} - \boldsymbol{e}_{np}^{kT} \boldsymbol{\mathscr{E}}_{nG}^{k} - \boldsymbol{\lambda}_{p}^{k} \theta^{k}, \tag{64}$$

$$\boldsymbol{\sigma}_{nC}^{k} = \boldsymbol{Q}_{np}^{k} \boldsymbol{\epsilon}_{pG}^{k} + \boldsymbol{Q}_{nn}^{k} \boldsymbol{\epsilon}_{nG}^{k} - \boldsymbol{e}_{pn}^{kT} \boldsymbol{\mathscr{E}}_{pG}^{k} - \boldsymbol{e}_{nn}^{kT} \boldsymbol{\mathscr{E}}_{nG}^{k} - \boldsymbol{\lambda}_{n}^{k} \theta^{k}, \tag{65}$$

$$\boldsymbol{\mathscr{D}}_{pC}^{k} = \boldsymbol{e}_{pp}^{k} \boldsymbol{\epsilon}_{pG}^{k} + \boldsymbol{e}_{pn}^{k} \boldsymbol{\epsilon}_{nG}^{k} + \boldsymbol{\varepsilon}_{pp}^{k} \boldsymbol{\mathscr{E}}_{pG}^{k} + \boldsymbol{\varepsilon}_{pn}^{k} \boldsymbol{\mathscr{E}}_{nG}^{k} + \boldsymbol{p}_{p}^{k} \theta^{k}, \tag{66}$$

$$\boldsymbol{\mathscr{D}}_{nC}^{k} = \boldsymbol{e}_{np}^{k} \boldsymbol{\epsilon}_{pG}^{k} + \boldsymbol{e}_{nn}^{k} \boldsymbol{\epsilon}_{nG}^{k} + \boldsymbol{\varepsilon}_{np}^{k} \boldsymbol{\mathscr{E}}_{pG}^{k} + \boldsymbol{\varepsilon}_{nn}^{k} \boldsymbol{\mathscr{E}}_{nG}^{k} + \boldsymbol{p}_{n}^{k} \theta^{k}, \tag{67}$$

$$\eta_{C}^{k} = \boldsymbol{\lambda}_{p}^{kT} \boldsymbol{\epsilon}_{pG}^{k} + \boldsymbol{\lambda}_{n}^{kT} \boldsymbol{\epsilon}_{nG}^{k} + \boldsymbol{p}_{p}^{kT} \boldsymbol{\mathscr{E}}_{pG}^{k} + \boldsymbol{p}_{n}^{kT} \boldsymbol{\mathscr{E}}_{nG}^{k} + \chi^{k} \theta^{k}. \tag{68}$$

The geometrical relations for plates have already been obtained, Carrera Unified Formulation has been described earlier. Eq. (63) is rewritten in the following form for a generic k layer:

$$\int_{\Omega_k} \int_{A_k} \Big[\Big(\boldsymbol{D}_p F_s \delta \boldsymbol{u}_s^k \Big)^T \Big(\big(\boldsymbol{Q}_{pp}^k \boldsymbol{D}_p + \boldsymbol{Q}_{pn}^k (\boldsymbol{D}_{np} + \boldsymbol{D}_{nz}) \big) F_\tau \boldsymbol{u}_\tau^k$$
$$+ \boldsymbol{e}_{pp}^{kT} \boldsymbol{D}_{ep} F_\tau \Phi_\tau^k + \boldsymbol{e}_{np}^{kT} \boldsymbol{D}_{en} F_\tau \Phi_\tau^k - \boldsymbol{\lambda}_p^k F_\tau \theta_\tau^k \Big) + \Big((\boldsymbol{D}_{np} + \boldsymbol{D}_{nz}) F_s \delta \boldsymbol{u}_s^k \Big)^T$$
$$\times \Big(\big(\boldsymbol{Q}_{np}^k \boldsymbol{D}_p + \boldsymbol{Q}_{nn}^k (\boldsymbol{D}_{np} + \boldsymbol{D}_{nz}) \big) F_\tau \boldsymbol{u}_\tau^k + \boldsymbol{e}_{pn}^{kT} \boldsymbol{D}_{ep} F_\tau \Phi_\tau^k$$
$$+ \boldsymbol{e}_{nn}^{kT} \boldsymbol{D}_{en} F_\tau \Phi_\tau^k - \boldsymbol{\lambda}_n^k F_\tau \theta_\tau^k \Big) + \Big(\boldsymbol{D}_{ep} F_s \delta \Phi_s^k \Big)^T \Big(\big(\boldsymbol{e}_{pp}^k \boldsymbol{D}_p + \boldsymbol{e}_{pn}^k (\boldsymbol{D}_{np} + \boldsymbol{D}_{nz}) \big)$$
$$\times F_\tau \boldsymbol{u}_\tau^k - \boldsymbol{\varepsilon}_{pp}^k \boldsymbol{D}_{ep} F_\tau \Phi_\tau^k - \boldsymbol{\varepsilon}_{pn}^k \boldsymbol{D}_{en} F_\tau \Phi_\tau^k + \boldsymbol{p}_p^k F_\tau \theta_\tau^k \Big) + \Big(\boldsymbol{D}_{en} F_s \delta \Phi_s^k \Big)^T$$
$$\times \Big(\big(\boldsymbol{e}_{np}^k \boldsymbol{D}_p + \boldsymbol{e}_{nn}^k (\boldsymbol{D}_{np} + \boldsymbol{D}_{nz}) \big) F_\tau \boldsymbol{u}_\tau^k - \boldsymbol{\varepsilon}_{np}^k \boldsymbol{D}_{ep} F_\tau \Phi_\tau^k - \boldsymbol{\varepsilon}_{nn}^k \boldsymbol{D}_{en} F_\tau \Phi_\tau^k + \boldsymbol{p}_n^k F_\tau \theta_\tau^k \Big)$$
$$- F_s \delta \theta_s^{kT} \Big(\big(\boldsymbol{\lambda}_p^{kT} \boldsymbol{D}_p + \boldsymbol{\lambda}_n^{kT} (\boldsymbol{D}_{np} + \boldsymbol{D}_{nz}) \big) F_\tau \boldsymbol{u}_\tau^k - \boldsymbol{p}_p^{kT} \boldsymbol{D}_{ep} F_\tau \Phi_\tau^k - \boldsymbol{p}_n^{kT} \boldsymbol{D}_{en} F_\tau \Phi_\tau^k + \chi^k F_\tau \theta_\tau^k \Big) \Big]$$
$$d\Omega_k \, dz = \delta L_e^k - \delta L_{in}^k. \tag{69}$$

Integrating by parts the Eq. (69) (as suggested in [5] and [6]), the fundamental nuclei are obtained via comparison with the governing relations in Eqs. (61):

$$\boldsymbol{K}_{uu}^{k\tau s} = \int_{A_k} \Big[\Big(-\boldsymbol{D}_p \Big)^T \Big(\boldsymbol{Q}_{pp}^k \boldsymbol{D}_p + \boldsymbol{Q}_{pn}^k (\boldsymbol{D}_{np} + \boldsymbol{D}_{nz}) \Big) + \Big(-\boldsymbol{D}_{np} + \boldsymbol{D}_{nz} \Big)^T \Big(\boldsymbol{Q}_{np}^k \boldsymbol{D}_p + \boldsymbol{Q}_{nn}^k (\boldsymbol{D}_{np} + \boldsymbol{D}_{nz}) \Big) \Big] F_s F_\tau dz, \tag{70}$$

$$\boldsymbol{K}_{u\Phi}^{k\tau s} = \int_{A_k} \Big[\Big(-\boldsymbol{D}_p \Big)^T \Big(\boldsymbol{e}_{pp}^{kT} \boldsymbol{D}_{ep} + \boldsymbol{e}_{np}^{kT} \boldsymbol{D}_{en} \Big) + \Big(-\boldsymbol{D}_{np} + \boldsymbol{D}_{nz} \Big)^T \Big(\boldsymbol{e}_{pn}^{kT} \boldsymbol{D}_{ep} + \boldsymbol{e}_{nn}^{kT} \boldsymbol{D}_{en} \Big) \Big] F_s F_\tau dz, \tag{71}$$

$$\boldsymbol{K}_{u\theta}^{k\tau s} = \int_{A_k} \Big[\Big(-\boldsymbol{D}_p \Big)^T \Big(-\boldsymbol{\lambda}_p^k \Big) + \Big(-\boldsymbol{D}_{np} + \boldsymbol{D}_{nz} \Big)^T \Big(-\boldsymbol{\lambda}_n^k \Big) \Big] F_s F_\tau dz, \tag{72}$$

$$\boldsymbol{K}_{\Phi u}^{k\tau s} = \int_{A_k} \Big[\Big(-\boldsymbol{D}_{ep} \Big)^T \Big(\boldsymbol{e}_{pp}^k \boldsymbol{D}_p + \boldsymbol{e}_{pn}^k \Big(\boldsymbol{D}_{np} + \boldsymbol{D}_{nz} \Big) \Big) + \Big(\boldsymbol{D}_{en} \Big)^T \Big(\boldsymbol{e}_{np}^k \boldsymbol{D}_p + \boldsymbol{e}_{nn}^k \Big(\boldsymbol{D}_{np} + \boldsymbol{D}_{nz} \Big) \Big) \Big] F_s F_\tau dz, \tag{73}$$

$$\boldsymbol{K}_{\Phi\Phi}^{k\tau s} = \int_{A_k} \Big[\Big(\boldsymbol{D}_{ep} \Big)^T \Big(\boldsymbol{\varepsilon}_{pp}^k \boldsymbol{D}_{ep} + \boldsymbol{\varepsilon}_{pn}^k \boldsymbol{D}_{en} \Big) - \Big(\boldsymbol{D}_{en} \Big)^T \Big(\boldsymbol{\varepsilon}_{np}^k \boldsymbol{D}_{ep} + \boldsymbol{\varepsilon}_{nn}^k \boldsymbol{D}_{en} \Big) \Big] F_s F_\tau dz, \tag{74}$$

$$\boldsymbol{K}_{\Phi\theta}^{k\tau s} = \int_{A_k} \Big[-\boldsymbol{D}_{ep}^T \boldsymbol{p}_p^k + \boldsymbol{D}_{en}^T \boldsymbol{p}_n^k \Big] F_s F_\tau dz, \tag{75}$$

$$\boldsymbol{K}_{\theta u}^{k\tau s} = \int_{A_k} \Big[-\boldsymbol{\lambda}_p^{kT} \boldsymbol{D}_p - \boldsymbol{\lambda}_n^{kT} \Big(\boldsymbol{D}_{np} + \boldsymbol{D}_{nz} \Big) \Big] F_s F_\tau dz, \tag{76}$$

$$\boldsymbol{K}_{\theta\Phi}^{k\tau s} = \int_{A_k} \Big[\boldsymbol{p}_p^{kT} \boldsymbol{D}_{ep} + \boldsymbol{p}_n^{kT} \boldsymbol{D}_{en} \Big] F_s F_\tau dz, \tag{77}$$

$$\boldsymbol{K}_{\theta\theta}^{k\tau s} = \int_{A_k} -\chi^k F_s F_\tau dz. \tag{78}$$

The nuclei for boundary conditions on the edge Γ_k are:

$$\boldsymbol{\Pi}_{uu}^{k\tau s} = \int_{A_k} \Big[\boldsymbol{I}_p^T \Big(\boldsymbol{Q}_{pp}^k \boldsymbol{D}_p + \boldsymbol{Q}_{pn}^k (\boldsymbol{D}_{np} + \boldsymbol{D}_{nz}) \Big) + \boldsymbol{I}_{np}^T \Big(\boldsymbol{Q}_{np}^k \boldsymbol{D}_p + \boldsymbol{Q}_{nn}^k (\boldsymbol{D}_{np} + \boldsymbol{D}_{nz}) \Big) \Big] F_s F_\tau dz, \tag{79}$$

$$\boldsymbol{\Pi}_{u\Phi}^{k\tau s} = \int_{A_k} \Big[\boldsymbol{I}_p^T \Big(\boldsymbol{e}_{pp}^{kT} \boldsymbol{D}_{ep} + \boldsymbol{e}_{np}^{kT} \boldsymbol{D}_{en} \Big) + \boldsymbol{I}_{np}^T \Big(\boldsymbol{e}_{pn}^{kT} \boldsymbol{D}_{ep} + \boldsymbol{e}_{nn}^{kT} \boldsymbol{D}_{en} \Big) \Big] F_s F_\tau dz, \tag{80}$$

$$\boldsymbol{\Pi}_{u\theta}^{k\tau s} = \int_{A_k} \Big[-\boldsymbol{I}_p^T \boldsymbol{\lambda}_p^k - \boldsymbol{I}_{np}^T \boldsymbol{\lambda}_n^k \Big] F_s F_\tau dz, \tag{81}$$

$$\boldsymbol{\Pi}_{\Phi u}^{k\tau s} = \int_{A_k} \Big[\boldsymbol{I}_{ep}^T \Big(\boldsymbol{e}_{pp}^k \boldsymbol{D}_p + \boldsymbol{e}_{pn}^k \Big(\boldsymbol{D}_{np} + \boldsymbol{D}_{nz} \Big) \Big) \Big] F_s F_\tau dz, \tag{82}$$

$$\boldsymbol{\Pi}_{\Phi\Phi}^{k\tau s} = \int_{A_k} \Big[-\boldsymbol{I}_{ep}^T \Big(\boldsymbol{\varepsilon}_{pp}^k \boldsymbol{D}_{ep} + \boldsymbol{\varepsilon}_{pn}^k \boldsymbol{D}_{en} \Big) \Big] F_s F_\tau dz, \tag{83}$$

$$\boldsymbol{\Pi}_{\Phi\theta}^{k\tau s} = \int_{A_k} \Big[\boldsymbol{I}_{ep}^T \boldsymbol{p}_p^k \Big] F_s F_\tau dz, \tag{84}$$

$$\boldsymbol{\Pi}^{k\tau s}_{\theta u} = 0, \tag{85}$$

$$\boldsymbol{\Pi}^{k\tau s}_{\theta\Phi} = 0, \tag{86}$$

$$\boldsymbol{\Pi}^{k\tau s}_{\theta\theta} = 0. \tag{87}$$

$\boldsymbol{I}_p$ and $\boldsymbol{I}_{np}$ are (3×3) matrices, used to perform the integration by parts, which are obtained from $\boldsymbol{D}_p$ and $\boldsymbol{D}_{np}$ simply replacing the differential operators with 1. $\boldsymbol{I}_{ep}$ has dimension (2×1), it also permits to perform the integration by parts and it is obtained from the matrix $\boldsymbol{D}_{ep}$ simply replacing the differential operators with 1. Nuclei, given in Eqs. (70)–(78), are introduced in the governing Eq. (61) in the case of mechanical load or electric potential applied on the plate surfaces. In this case, in Eq. (61) the inertial contribute and the thermal load are discarded. The electric potential is directly imposed in the vector Φ^k_τ; therefore, the electric load $\boldsymbol{p}^k_{\Phi s}$ is not considered. Nuclei for boundary conditions in Eqs. (79)–(87) are introduced in the boundary conditions of Eq. (62) in the case of applied mechanical load or imposed electric potential.

PVD for Imposed Temperature

In the case of temperature imposed on surfaces of the structure, the term $\delta\theta^k\eta^k_C$ in the Eq. (60) is not considered to allow the comparison with classical thermal stress analysis proposed in the open literature (the effects of such a term should be discussed in future works). Therefore, the variational statement is:

$$\sum_{k=1}^{N_l}\int_{\Omega_k}\int_{A_k}\left\{\delta\boldsymbol{\epsilon}^{k\,T}_{pG}\boldsymbol{\sigma}^k_{pC} + \delta\boldsymbol{\epsilon}^{k\,T}_{nG}\boldsymbol{\sigma}^k_{nC} - \delta\boldsymbol{\mathscr{E}}^{k\,T}_{pG}\boldsymbol{\mathscr{D}}^k_{pC} - \delta\boldsymbol{\mathscr{E}}^{k\,T}_{nG}\boldsymbol{\mathscr{D}}^k_{nC} - \delta\boldsymbol{\vartheta}^T_{pG}\boldsymbol{h}_{pC} - \delta\boldsymbol{\vartheta}^T_{nG}\boldsymbol{h}_{nC}\right\}$$

$$d\Omega_k dz = \sum_{k=1}^{N_l}\delta L^k_e - \sum_{k=1}^{N_l}\delta L^k_{in}. \tag{88}$$

The constitutive equations are obtained from Eqs. (27)–(33) simply discarding the entropy η^k_c:

$$\boldsymbol{\sigma}^k_{pC} = \boldsymbol{Q}^k_{pp}\boldsymbol{\epsilon}^k_{pG} + \boldsymbol{Q}^k_{pn}\boldsymbol{\epsilon}^k_{nG} - \boldsymbol{e}^{kT}_{pp}\boldsymbol{\mathscr{E}}^k_{pG} - \boldsymbol{e}^{kT}_{np}\boldsymbol{\mathscr{E}}^k_{nG} - \boldsymbol{\lambda}^k_p\theta^k, \tag{89}$$

$$\boldsymbol{\sigma}^k_{nC} = \boldsymbol{Q}^k_{np}\boldsymbol{\epsilon}^k_{pG} + \boldsymbol{Q}^k_{nn}\boldsymbol{\epsilon}^k_{nG} - \boldsymbol{e}^{kT}_{pn}\boldsymbol{\mathscr{E}}^k_{pG} - \boldsymbol{e}^{kT}_{nn}\boldsymbol{\mathscr{E}}^k_{nG} - \boldsymbol{\lambda}^k_n\theta^k, \tag{90}$$

$$\boldsymbol{\mathscr{D}}^k_{pC} = \boldsymbol{e}^k_{pp}\boldsymbol{\epsilon}^k_{pG} + \boldsymbol{e}^k_{pn}\boldsymbol{\epsilon}^k_{nG} + \boldsymbol{\varepsilon}^k_{pp}\boldsymbol{\mathscr{E}}^k_{pG} + \boldsymbol{\varepsilon}^k_{pn}\boldsymbol{\mathscr{E}}^k_{nG} + \boldsymbol{p}^k_p\theta^k, \tag{91}$$

$$\boldsymbol{\mathscr{D}}^k_{nC} = \boldsymbol{e}^k_{np}\boldsymbol{\epsilon}^k_{pG} + \boldsymbol{e}^k_{nn}\boldsymbol{\epsilon}^k_{nG} + \boldsymbol{\varepsilon}^k_{np}\boldsymbol{\mathscr{E}}^k_{pG} + \boldsymbol{\varepsilon}^k_{nn}\boldsymbol{\mathscr{E}}^k_{nG} + \boldsymbol{p}^k_n\theta^k, \tag{92}$$

$$\boldsymbol{h}^k_p = \boldsymbol{\kappa}^k_{pp}\boldsymbol{\vartheta}^k_{pG} + \boldsymbol{\kappa}^k_{pn}\boldsymbol{\vartheta}^k_{nG}, \tag{93}$$

$$\boldsymbol{h}^k_n = \boldsymbol{\kappa}^k_{np}\boldsymbol{\vartheta}^k_{pG} + \boldsymbol{\kappa}^k_{nn}\boldsymbol{\vartheta}^k_{nG}. \tag{94}$$

The geometrical relations for plates have been obtained previously and the Carrera Unified Formulation has been described earlier. Eq. (88) is rewritten in the following

form for a generic k layer:

$$\int_{\Omega_k}\int_{A_k}\Big[\Big(\boldsymbol{D}_p F_s\delta\boldsymbol{u}_s^k\Big)^T\Big(\big(\boldsymbol{Q}_{pp}^k\boldsymbol{D}_p+\boldsymbol{Q}_{pn}^k(\boldsymbol{D}_{np}+\boldsymbol{D}_{nz})\big)F_\tau\boldsymbol{u}_\tau^k + \boldsymbol{e}_{pp}^{kT}\boldsymbol{D}_{ep}F_\tau\Phi_\tau^k+\boldsymbol{e}_{np}^{kT}\boldsymbol{D}_{en}F_\tau\Phi_\tau^k-\boldsymbol{\lambda}_p^kF_\tau\theta_\tau^k\Big)+\Big(\big(\boldsymbol{D}_{np}+\boldsymbol{D}_{nz}\big)F_s\delta\boldsymbol{u}_s^k\Big)^T \times\Big(\big(\boldsymbol{Q}_{np}^k\boldsymbol{D}_p+\boldsymbol{Q}_{nn}^k(\boldsymbol{D}_{np}+\boldsymbol{D}_{nz})\big)F_\tau\boldsymbol{u}_\tau^k+\boldsymbol{e}_{pn}^{kT}\boldsymbol{D}_{ep}F_\tau\Phi_\tau^k+\boldsymbol{e}_{nn}^{kT}\boldsymbol{D}_{en}F_\tau\Phi_\tau^k-\boldsymbol{\lambda}_n^kF_\tau\theta_\tau^k\Big) +\Big(\boldsymbol{D}_{ep}F_s\delta\Phi_s^k\Big)^T\Big(\big(\boldsymbol{e}_{pp}^k\boldsymbol{D}_p+\boldsymbol{e}_{pn}^k(\boldsymbol{D}_{np}+\boldsymbol{D}_{nz})\big) \times F_\tau\boldsymbol{u}_\tau^k-\boldsymbol{\varepsilon}_{pp}^k\boldsymbol{D}_{ep}F_\tau\Phi_\tau^k-\boldsymbol{\varepsilon}_{pn}^k\boldsymbol{D}_{en}F_\tau\Phi_\tau^k+\boldsymbol{p}_p^kF_\tau\theta_\tau^k\Big) +\Big(\boldsymbol{D}_{en}F_s\delta\Phi_s^k\Big)^T\Big(\big(\boldsymbol{e}_{np}^k\boldsymbol{D}_p+\boldsymbol{e}_{nn}^k(\boldsymbol{D}_{np}+\boldsymbol{D}_{nz})\big) \times F_\tau\boldsymbol{u}_\tau^k-\boldsymbol{\varepsilon}_{np}^k\boldsymbol{D}_{ep}F_\tau\Phi_\tau^k-\boldsymbol{\varepsilon}_{nn}^k\boldsymbol{D}_{en}F_\tau\Phi_\tau^k+\boldsymbol{p}_n^kF_\tau\theta_\tau^k\Big) +\Big(\boldsymbol{D}_{tp}F_s\delta\theta_s^k\Big)^T\Big(-\boldsymbol{\kappa}_{pp}^k\boldsymbol{D}_{tp}F_\tau\theta_\tau^k-\boldsymbol{\kappa}_{pn}^k\boldsymbol{D}_{tn}F_\tau\theta_\tau^k\Big) +\Big(\boldsymbol{D}_{tn}F_s\delta\theta_s^k\Big)^T\Big(-\boldsymbol{\kappa}_{np}^k\boldsymbol{D}_{tp}F_\tau\theta_\tau^k-\boldsymbol{\kappa}_{nn}^k\boldsymbol{D}_{tn}F_\tau\theta_\tau^k\Big)\Big] d\Omega_k\,dz=\delta L_e^k-\delta L_{in}^k. \tag{95}$$

Integrating by parts the Eq. (95) (see [5] and [6]), the fundamental nuclei $\boldsymbol{K}_{uu}^{k\tau s}$, $\boldsymbol{K}_{u\Phi}^{k\tau s}$, $\boldsymbol{K}_{u\theta}^{k\tau s}$, $\boldsymbol{K}_{\Phi u}^{k\tau s}$, $\boldsymbol{K}_{\Phi\Phi}^{k\tau s}$ and $\boldsymbol{K}_{\Phi\theta}^{k\tau s}$ are the same of PVD already seen for the applied mechanical load or imposed electric potential, while nuclei $\boldsymbol{K}_{\theta u}^{k\tau s}$, $\boldsymbol{K}_{\theta\Phi}^{k\tau s}$ and $\boldsymbol{K}_{\theta\theta}^{k\tau s}$ are:

$$\boldsymbol{K}_{\theta u}^{k\tau s}=0, \tag{96}$$

$$\boldsymbol{K}_{\theta\Phi}^{k\tau s}=0, \tag{97}$$

$$\boldsymbol{K}_{\theta\theta}^{k\tau s}=\int_{A_k}\Big[\Big(\boldsymbol{D}_{tp}\Big)^T\Big(\boldsymbol{\kappa}_{pp}^k\boldsymbol{D}_{tp}+\boldsymbol{\kappa}_{pn}^k\boldsymbol{D}_{tn}\Big)-\Big(\boldsymbol{D}_{tn}\Big)^T\Big(\boldsymbol{\kappa}_{np}^k\boldsymbol{D}_{tp}+\boldsymbol{\kappa}_{nn}^k\boldsymbol{D}_{tn}\Big)\Big]F_sF_\tau dz. \tag{98}$$

Nuclei for boundary conditions on the edge Γ_k $\boldsymbol{\Pi}_{uu}^{k\tau s}$, $\boldsymbol{\Pi}_{u\Phi}^{k\tau s}$, $\boldsymbol{\Pi}_{u\theta}^{k\tau s}$, $\boldsymbol{\Pi}_{\Phi u}^{k\tau s}$, $\boldsymbol{\Pi}_{\Phi\Phi}^{k\tau s}$, $\boldsymbol{\Pi}_{\Phi\theta}^{k\tau s}$, $\boldsymbol{\Pi}_{\theta u}^{k\tau s}$ and $\boldsymbol{\Pi}_{\theta\Phi}^{k\tau s}$ are the same of PVD previously described for the applied mechanical load or imposed electric potential, while nucleus $\boldsymbol{\Pi}_{\theta\theta}^{k\tau s}$ is different:

$$\boldsymbol{\Pi}_{\theta\theta}^{k\tau s}=\int_{A_k}\Big[\Big(-\boldsymbol{I}_{tp}\Big)^T\Big(\boldsymbol{\kappa}_{pp}^k\boldsymbol{D}_{tp}+\boldsymbol{\kappa}_{pn}^k\boldsymbol{D}_{tn}\Big)\Big]F_sF_\tau dz, \tag{99}$$

where $\boldsymbol{I}_{tp}$ has dimension (2×1), it allows the integration by parts to be performed and it is obtained from the matrix $\boldsymbol{D}_{tp}$ simply replacing the differential operators with 1. Nuclei, here obtained, are introduced in the governing Eq. (61) in the case of imposed temperature on the surfaces. In this case, in Eq. (61) the mechanical and electrical loads, and the inertial contribute are discarded. The temperature is directly imposed in the vector θ_τ^k; therefore, the thermal load $\boldsymbol{p}_{\theta s}^k$ is not considered. Nuclei for boundary conditions here discussed are introduced in the boundary conditions of Eq. (62) in the case of imposed temperature on the surfaces.

NAVIER SOLUTION AND ASSEMBLING PROCEDURE

To write the explicit form of fundamental nuclei obtained earlier, the following integrals in the z-thickness direction must be defined:

$$(J^{k\tau s}, J^{k\tau_z s}, J^{k\tau s_z}, J^{k\tau_z s_z}) = \int_{A_k} \left(F_\tau F_s, \frac{\partial F_\tau}{\partial z} F_s, F_\tau \frac{\partial F_s}{\partial z}, \frac{\partial F_\tau}{\partial z} \frac{\partial F_s}{\partial z} \right) dz. \tag{100}$$

The explicit forms of fundamental nuclei are obtained by using the Eqs. (100) and developing the matrices products.

Navier-type closed-form solution is obtained via substitution of harmonic expressions for the displacements, electric potential and temperature as well as considering the following material coefficients equal zero: $Q_{16} = Q_{26} = Q_{36} = Q_{45} = 0$, $\varepsilon_{12} = p_1 = p_2 = e_{25} = e_{14} = e_{36} = 0$ and $\lambda_6 = \kappa_{12} = 0$. The following harmonic assumptions can be made for the variables, which correspond to simply supported boundary conditions:

$$\begin{aligned}
u_\tau^k &= \sum_{m,n} (\widehat{U}_\tau^k) \cos\left(\frac{m\pi x}{a}\right) \sin\left(\frac{n\pi y}{b}\right), \quad k = 1, N_l, \\
v_\tau^k &= \sum_{m,n} (\widehat{V}_\tau^k) \sin\left(\frac{m\pi x}{a}\right) \cos\left(\frac{n\pi y}{b}\right), \quad \tau = t, b, r, \\
(w_\tau^k, \Phi_\tau^k, \theta_\tau^k) &= \sum_{m,n} (\widehat{W}_\tau^k, \hat{\Phi}_\tau^k, \hat{\theta}_\tau^k) \sin\left(\frac{m\pi x}{a}\right) \sin\left(\frac{n\pi y}{b}\right), \quad r = 2, N,
\end{aligned} \tag{101}$$

where $\widehat{U}_\tau^k$, $\widehat{V}_\tau^k$, $\widehat{W}_\tau^k$, $\hat{\Phi}_\tau^k$, $\hat{\theta}_\tau^k$ are the amplitudes.

Fundamental nucleus $\boldsymbol{K}_{uu}^{k\tau s}$, of dimension (3×3), is in common for each considered case:

$$\begin{aligned}
&K_{uu_{11}}^{k\tau s} = Q_{55}^k J^{k\tau_z s_z} + Q_{11}^k J^{k\tau s} \bar{\alpha}^2 + Q_{66}^k J^{k\tau s} \bar{\beta}^2, \quad K_{uu_{12}}^{k\tau s} = J^{k\tau s} \bar{\alpha}\bar{\beta} (Q_{12}^k + Q_{66}^k) = K_{uu_{21}}^{k\tau s}, \\
&K_{uu_{13}}^{k\tau s} = Q_{55}^k J^{k\tau_z s} \bar{\alpha} - Q_{13}^k J^{k\tau s_z} \bar{\alpha}, \quad K_{uu_{22}}^{k\tau s} = Q_{44}^k J^{k\tau_z s_z} + Q_{22}^k J^{k\tau s} \bar{\beta}^2 + Q_{66}^k J^{k\tau s} \bar{\alpha}^2, \\
&K_{uu_{23}}^{k\tau s} = Q_{44}^k J^{k\tau_z s} \bar{\beta} - Q_{23}^k J^{k\tau s_z} \bar{\beta}, \quad K_{uu_{31}}^{k\tau s} = Q_{55}^k J^{k\tau s_z} \bar{\alpha} - Q_{13}^k J_\beta^{k\tau_z s} \bar{\alpha}, \\
&K_{uu_{32}}^{k\tau s} = Q_{44}^k J^{k\tau s_z} \bar{\beta} - Q_{23}^k J^{k\tau_z s} \bar{\beta}, \quad K_{uu_{33}}^{k\tau s} = Q_{55}^k J^{k\tau s} \bar{\alpha}^2 + Q_{44}^k J^{k\tau s} \bar{\beta}^2 + Q_{33}^k J^{k\tau_z s_z}.
\end{aligned} \tag{102}$$

Fundamental nucleus $\boldsymbol{K}_{u\Phi}^{k\tau s}$, of dimension (3×1), is in common for each considered case:

$$\begin{aligned}
&K_{u\Phi_{11}}^{k\tau s} = \bar{\alpha} J^{k\tau_z s} e_{15}^k - \bar{\alpha} J^{k\tau s_z} e_{31}^k, \quad K_{u\Phi_{21}}^{k\tau s} = \bar{\beta} J^{k\tau_z s} e_{24}^k - \bar{\beta} J^{k\tau s_z} e_{32}^k, \\
&K_{u\Phi_{31}}^{k\tau s} = \bar{\alpha}^2 J^{k\tau s} e_{15}^k + J^{k\tau_z s_z} e_{33}^k + \bar{\beta}^2 J^{k\tau s} e_{24}^k.
\end{aligned} \tag{103}$$

Fundamental nucleus $\boldsymbol{K}_{u\theta}^{k\tau s}$, of dimension (3×1), is in common for each considered case:

$$K_{u\theta_{11}}^{k\tau s} = \bar{\alpha} J^{k\tau s} \lambda_1^k, \quad K_{u\theta_{21}}^{k\tau s} = \bar{\beta} J^{k\tau s} \lambda_2^k, \quad K_{u\theta_{31}}^{k\tau s} = -J^{k\tau_z s} \lambda_3^k. \tag{104}$$

Fundamental nucleus $\boldsymbol{K}_{\Phi u}^{k\tau s}$, of dimension (1×3), is in common for each considered case:

$$K_{\Phi u_{11}}^{k\tau s} = \bar{\alpha} J^{k\tau s_z} e_{15}^k - \bar{\alpha} J^{k\tau_z s} e_{31}^k, \quad K_{\Phi u_{12}}^{k\tau s} = \bar{\beta} J^{k\tau s_z} e_{24}^k - \bar{\beta} J^{k\tau_z s} e_{32}^k, \tag{105}$$
$$K_{\Phi u_{13}}^{k\tau s} = \bar{\alpha}^2 J^{k\tau s} e_{15}^k + J^{k\tau_z s_z} e_{33}^k + \bar{\beta}^2 J^{k\tau s} e_{24}^k.$$

Fundamental nucleus $\boldsymbol{K}_{\Phi\Phi}^{k\tau s}$, of dimension (1×1), is in common for each considered case:

$$K_{\Phi\Phi_{11}}^{k\tau s} = -\bar{\alpha}^2 J^{k\tau s} \varepsilon_{11}^k - J^{k\tau_z s_z} \varepsilon_{33}^k - \bar{\beta}^2 J^{k\tau s} \varepsilon_{22}^k. \tag{106}$$

Fundamental nucleus $\boldsymbol{K}_{\Phi\theta}^{k\tau s}$, of dimension (1×1), is in common for each considered case:

$$K_{\Phi\theta_{11}}^{k\tau s} = J^{k\tau_z s} p_3^k. \tag{107}$$

Fundamental nucleus $\boldsymbol{K}_{\theta u}^{k\tau s}$, of dimension (1×3) for the case of applied mechanical load or imposed electric potential is:

$$K_{\theta u_{11}}^{k\tau s} = \bar{\alpha} J^{k\tau s} \lambda_1^k, \quad K_{\theta u_{12}}^{k\tau s} = \bar{\beta} J^{k\tau s} \lambda_2^k, \quad K_{\theta u_{13}}^{k\tau s} = -J^{k\tau s_z} \lambda_3^k. \tag{108}$$

Fundamental nucleus $\boldsymbol{K}_{\theta u}^{k\tau s}$, of dimension (1×3) for the case of a imposed temperature has all zero components:

$$K_{\theta u_{11}}^{k\tau s} = K_{\theta u_{12}}^{k\tau s} = K_{\theta u_{13}}^{k\tau s} = 0. \tag{109}$$

Fundamental nucleus $\boldsymbol{K}_{\theta\Phi}^{k\tau s}$, of dimension (1×1), for the case of applied mechanical load or imposed electric potential is:

$$K_{\theta\Phi_{11}}^{k\tau s} = J^{k\tau s_z} p_3^k. \tag{110}$$

Fundamental nucleus $\boldsymbol{K}_{\theta\Phi}^{k\tau s}$, of dimension (1×1) for the case of a imposed temperature has zero component:

$$K_{\theta\Phi_{11}}^{k\tau s} = 0. \tag{111}$$

Fundamental nucleus $\boldsymbol{K}_{\theta\theta}^{k\tau s}$, of dimension (1×1), for the case of applied mechanical load or imposed electric potential is:

$$K_{\theta\theta_{11}}^{k\tau s} = -\chi^k J^{k\tau s}. \tag{112}$$

Fundamental nucleus $\boldsymbol{K}_{\theta\theta}^{k\tau s}$, of dimension (1×1), for the case of imposed temperature is:

$$K_{\theta\theta_{11}}^{k\tau s} = -\bar{\alpha}^2 \kappa_{11}^k J^{k\tau s} - \bar{\beta}^2 \kappa_{22}^k J^{k\tau s} - \kappa_{33}^k J^{k\tau_z s_z}. \tag{113}$$

In each proposed fundamental nucleus the derivatives give the terms $\bar{\alpha} = m\pi/a$ and $\bar{\beta} = n\pi/b$, where m and n are the wave numbers in in-plane directions, and a and b are the plate dimensions.

Matrices can be obtained for the considered multilayered plates by simply expanding and assembling the fundamental nuclei described in this section (via the indexes k, τ, s). The order of expansion N from 1 to 4 in the thickness direction is considered via indexes τ, s, these matrices are obtained for each considered layer. The index k allows the multilayer assembling procedure, which can either be ESL or LW.

ACRONYMS

A system of acronyms is here given in order to define the refined two-dimensional models developed in this work for the thermo-electro-mechanical analysis of multilayered plates. The choice made in this article is that displacements can be in ESL or LW form, but the electric potential and the sovra-temperature are always considered in LW form. Therefore, a two-dimensional model is defined as ESL or LW depending on the choice made for the displacement. ESL models are indicated as ED1-ED4, where E means the ESL approach, D means that the Principle of Virtual Displacements or their extensions to thermo-electro-mechanical analysis have been employed; the last digit, from 1 to 4, indicates the order of expansion in the thickness direction for displacements, electric potential and sovra-temperature. In the case of LW models, the letter E is replaced by a letter L; therefore, the relative models are indicated as LD1-LD4.

In the case of a multifield analysis, additional parentheses are introduced in the acronyms: (u,Φ,θ) means fully coupled thermo-electro-mechanical models, (u,Φ) is added in the case of fully coupled electro-mechanical analysis, (u,θ) is added in the case of fully coupled thermo-mechanical analysis and (u) means pure mechanical problem. The two-field and one-field models are simply obtained by deleting the opportune rows and columns in the governing Eq. (61), or by considering the opportune variational statement and constitutive equations where the thermal and/or electrical contributions are discarded.

RESULTS

The plates analyzed in this section are simply supported multilayered structures with applied mechanical or field loads in harmonic form. First, three assessments are proposed in order to validate the refined models for the cases of applied mechanical load, imposed electric potential and imposed sovra-temperature on the surfaces. The refined and classical models based on CUF theory are compared with well-known results given in the open literature [25, 30, 45]. Then, a new benchmark is analyzed where the importance of refined models is demonstrated if compared to classical ones and the effects of multifield coupling are deeply discussed. The benchmark considers three different loading cases in analogy with the preliminary assessments.

First Assessment, Mechanical Load

The simply supported square plate ($a = b$) has thickness ratio $S = a/h$ equals 5, 10 and 20 with total thickness $h = 1\,m$. A mechanical load is applied at the top surface in the z direction in the form $p_z = -p_0 sin(\frac{m\pi x}{a}) sin(\frac{n\pi y}{b})$ with $p_0 = 1\,Pa$ and wave numbers $m = n = 1$. The plate has free conditions at the surfaces for the electric potential Φ and for the sovra-temperature θ, in the case proposed by Kapuria and Nair [25] the interface between the piezoelectric layer and the composite one is grounded. The plate has five layers, four fiber-reinforced composite layers Gr/Ep with lamination sequence 0°/90°/90°/0° and thickness $h_1 = h_2 = h_3 = h_4 = 0.225\,h$, and a piezoelectric PZT5A layer at the top with thickness $h_5 = 0.1\,h$.

The Gr/Ep composite material has Young modulii $E_1 = 181\,GPa$ and $E_2 = E_3 = 10.3\,GPa$, shear modulii $G_{12} = G_{13} = 7.17\,GPa$ and $G_{23} = 2.87\,GPa$, Poisson ratios $\nu_{12} = \nu_{13} = 0.28$ and $\nu_{23} = 0.33$, mass density $\rho = 1578\,Kg/m^3$, specific heat per unit mass $C_v = 1409\,J/KgK$, coefficients of thermal expansion $\alpha_{11} = 0.02 \times 10^{-6}\,K^{-1}$ and $\alpha_{22} = \alpha_{33} = 22.5 \times 10^{-6}\,K^{-1}$, thermal conductivity coefficients $\kappa_{11} = 1.5\,W/mK$ and $\kappa_{22} = \kappa_{33} = 0.5\,W/mK$ and dielectric constants $\varepsilon_{11} = \varepsilon_{22} = \varepsilon_{33} = 1.53 \times 10^{-8}\,F/m$.

The piezoelectric material PZT5A has Young modulii $E_1 = E_2 = 61\,GPa$ and $E_3 = 53.2\,GPa$, shear modulii $G_{12} = 22.6\,GPa$ and $G_{23} = G_{13} = 21.1\,GPa$, Poisson ratios $\nu_{12} = 0.35$ and $\nu_{23} = \nu_{13} = 0.38$, mass density $\rho = 7600\,Kg/m^3$, specific heat per unit mass $C_v = 420\,J/KgK$, coefficients of thermal expansion $\alpha_{11} = \alpha_{22} = 1.5 \times 10^{-6}\,K^{-1}$ and $\alpha_{33} = 2 \times 10^{-6}\,K^{-1}$, thermal conductivity coefficients $\kappa_{11} = \kappa_{22} = \kappa_{33} = 1.8\,W/mK$, pyroelectric constant $p_3 = 0.0007\,C/m^2K$, piezoelectric coefficients $d_{31} = d_{32} = -171 \times 10^{-12}\,m/V$, $d_{33} = 374 \times 10^{-12}\,m/V$ and $d_{15} = d_{24} = 584 \times 10^{-12}\,m/V$ and dielectric constants $\varepsilon_{11} = \varepsilon_{22} = 1.53 \times 10^{-8}\,F/m$ and $\varepsilon_{33} = 1.5 \times 10^{-8}\,F/m$.

Refined and classical two-dimensional models based on CUF theory are compared with the 3D solution by Kapuria and Nair [25] in Tables 1, 2 and 3 for thickness ratios 5, 10 and 20, respectively. Displacements and stresses are given in no-dimensional form as $(\bar{u}, \bar{v}, \bar{w}) = 100(u, v, w/S)E_0/(hS^3 p_0)$ and $(\bar{\sigma}_{xx}, \bar{\sigma}_{yy}, \bar{\sigma}_{xz}) = (\sigma_{xx}, \sigma_{yy}, \sigma_{xz}S)/(S^2 p_0)$ with $E_0 = 10.3\,GPa$, they are evaluated at different positions through the thickness: the transverse displacements and the transverse shear stresses are given in the middle of the plate, the in-plane displacement is analyzed at the

Table 1 First assessment: Mechanical load applied to a multilayered composite plate embedding a piezoelectric layer

	$\bar{v}(-0.5h)$	$\bar{w}(0)$	$\bar{\sigma}_{xx}(0.4h^-)$	$\bar{\sigma}_{yy}(0.4h^+)$	$\bar{\sigma}_{xz}(0)$
3D [25]	−1.4407	−1.1485	−0.2977	−0.2600	−0.2346
LD4(u, Φ, θ)	−1.4403	−1.1486	−0.2974	−0.2601	−0.2346
ED4(u, Φ, θ)	−1.3830	−1.0934	−0.2780	−0.3178	−0.2051
FSDT(u, Φ, θ)	−0.9473	−0.8030	−0.2668	−0.2952	−0.0857
CLT(u, Φ, θ)	−0.7820	−0.4699	−0.3132	−0.2555	\
LD4(u, Φ)	−1.4405	−1.1488	−0.2975	−0.2601	−0.2346
LD4(u, θ)	−1.4786	−1.1856	−0.3255	−0.2346	−0.2394
LD4(u)	−1.4787	−1.1856	−0.3255	−0.2346	−0.2394

Comparison between classical, refined and three-dimensional models for the thickness ratio $a/h = 5$. The non-dimensional values are the maximum amplitudes in the plane.

Table 2 First assessment: Mechanical load applied to a multilayered composite plate embedding a piezoelectric layer

	$\bar{v}(-0.5h)$	$\bar{w}(0)$	$\bar{\sigma}_{xx}(0.4h^-)$	$\bar{\sigma}_{yy}(0.4h^+)$	$\bar{\sigma}_{xz}(0)$
3D [25]	−1.0202	−0.6802	−0.3196	−0.2424	−0.2740
LD4(u, Φ, θ)	−1.0200	−0.6800	−0.3194	−0.2425	−0.2740
ED4(u, Φ, θ)	−1.0004	−0.6639	−0.3140	−0.2577	−0.2352
FSDT(u, Φ, θ)	−0.8309	−0.5592	−0.3039	−0.2606	−0.0908
CLT(u, Φ, θ)	−0.7820	−0.4699	−0.3132	−0.2555	\
LD4(u, Φ)	−1.0202	−0.6802	−0.3196	−0.2424	−0.2740
LD4(u, θ)	−1.0527	−0.7116	−0.3485	−0.2067	−0.2806
LD4(u)	−1.0527	−0.7116	−0.3485	−0.2067	−0.2806

Comparison between classical, refined and three-dimensional models for the thickness ratio $a/h = 10$. The non-dimensional values are the maximum amplitudes in the plane.

bottom of the structure, the in-plane normal stresses in x and y direction are evaluated at the bottom of the interface between the piezoelectric layer and the composite one and at the top of the same interface, respectively.

From Table 1 it is clear how the Layer-Wise (LW) theory with fourth order of expansion is very efficient for the evaluation of both displacements and stresses. The LD4(u,Φ,θ) considers a full coupling between the mechanical, electrical and thermal fields, when the thermal field effect is discarded the theory LD4(u,Φ) gives almost the same results because thermal effect is not important in such a problem (in fact, Kapuria and Nair [25] do not consider thermal coupling in their 3D solution for the case of applied mechanical load). On the contrary, if we discard the electric field effect, the LD4(u,θ) model gives bigger displacements because a part of the energy is not converted in electrical energy, this means that the electric field coupling must be considered in such problems. The LD4(u) gives the biggest displacements because both electrical and thermal field effects are discarded, obviously the thermal effect is less important.

The main conclusion is that the discarding of a physical field (electrical and/or thermal ones) gives a bigger displacement because a part of the energy given by

Table 3 First assessment: Mechanical load applied to a multilayered composite plate embedding a piezoelectric layer

	$\bar{v}(-0.5h)$	$\bar{w}(0)$	$\bar{\sigma}_{xx}(0.4h^-)$	$\bar{\sigma}_{yy}(0.4h^+)$	$\bar{\sigma}_{xz}(0)$
3D [25]	−0.8764	−0.5488	−0.3323	−0.2302	−0.2893
LD4(u, Φ, θ)	−0.8763	−0.5487	−0.3322	−0.2303	−0.2892
ED4(u, Φ, θ)	−0.8708	−0.5444	−0.3302	−0.2360	−0.2465
FSDT(u, Φ, θ)	−0.7923	−0.4959	−0.3155	−0.2502	−0.0924
CLT(u, Φ, θ)	−0.7820	−0.4699	−0.3132	−0.2555	\
LD4(u, Φ)	−0.8764	−0.5488	−0.3323	−0.2302	−0.2893
LD4(u, θ)	−0.9056	−0.5778	−0.3613	−0.1922	−0.2964
LD4(u)	−0.9056	−0.5778	−0.3613	−0.1922	−0.2964

Comparison between classical, refined and three-dimensional models for the thickness ratio $a/h = 20$. The non-dimensional values are the maximum amplitudes in the plane

the mechanical load is not converted in thermal and/or electrical energy, moreover the effect of the electrical field is much more important than the effect of the thermal field for such a problem, similar conclusions can be given for the stress components. A comparison can be made between the LW model LD4(u,Φ,θ), the ESL model ED4(u,Φ,θ) and the classical ones FSDT(u,Φ,θ) and CLT(u,Φ,θ) by considering the fully coupling between the three physical fields. Classical models are completely inadequate and they give big errors, moreover CLT(u,Φ,θ) does not give any evaluation of the transverse shear stresses because they are zero in this theory as hypothesis.

The introduction of higher orders of expansion in ED4(u,Φ,θ) gives better results but the use of an ESL approach remains a limiting factor if compared with a LW model. In Tables 2 and 3 the thickness of the plate is smaller, in this case the differences between LW models and the ESL and classical ones are smaller but the use of LW theories remains mandatory to obtain a quasi-3D description of the smart plate in terms of displacements and stresses. In the present assessment, the LD4(u,Φ,θ) model is very close to the 3D solution by Kapuria and Nair [25] for each thickness ratio and it can be used as a reference solution in future benchmarks in the case of applied mechanical loads.

Second Assessment, Imposed Electric Potential

The simply supported square plate ($a = b$) has thickness ratio $S = a/h$ equals 4 with total thickness $h = 0.1\,m$. An electric voltage is applied at the top surface in the form $\Phi = \Phi_t sin(\frac{m\pi x}{a}) sin(\frac{n\pi y}{b})$ with $\Phi_t = 1\,V$ and wave numbers $m = n = 1$. The bottom of the plate has the electric potential imposed to zero ($\Phi_b = 0\,V$). The plate has free conditions at the surfaces for the sovra-temperature θ, in the case proposed by Heyliger [45] the thermal field effect is not considered because only the electro-mechanical coupling is investigated. Heyliger [45] proposed 3D results in terms of displacements, stresses and electric potential, such a variables are given at the top, middle and bottom of the multilayered smart structure. The plate has four layers, two internal fiber-reinforced composite layers Gr/Ep with lamination sequence 0°/90° and thickness $h_2 = h_3 = 0.4\,h$, and two external piezoelectric layers PZT4 with thickness $h_1 = h_4 = 0.1\,h$.

The Gr/Ep composite material has Young modulii $E_1 = 132.38\,GPa$ and $E_2 = E_3 = 10.756\,GPa$, shear modulii $G_{12} = G_{13} = 5.6537\,GPa$ and $G_{23} = 3.606\,GPa$, Poisson ratios $\nu_{12} = \nu_{13} = 0.24$ and $\nu_{23} = 0.49$, mass density $\rho = 1578\,Kg/m^3$, specific heat per unit mass $C_v = 1409\,J/KgK$, coefficients of thermal expansion $\alpha_{11} = 0.02 \times 10^{-6}\,K^{-1}$ and $\alpha_{22} = \alpha_{33} = 22.5 \times 10^{-6}\,K^{-1}$, thermal conductivity coefficients $\kappa_{11} = 1.5\,W/mK$ and $\kappa_{22} = \kappa_{33} = 0.5\,W/mK$ and dielectric constants $\varepsilon_{11} = 30.9897 \times 10^{-12}\,F/m$ and $\varepsilon_{22} = \varepsilon_{33} = 26.5626 \times 10^{-12}\,F/m$. The piezoelectric material PZT4 has Young modulii $E_1 = E_2 = 81.3\,GPa$ and $E_3 = 64.5\,GPa$, shear modulii $G_{12} = 30.6\,GPa$ and $G_{23} = G_{13} = 25.6\,GPa$, Poisson ratios $\nu_{12} = 0.329$ and $\nu_{23} = \nu_{13} = 0.432$, mass density $\rho = 7600\,Kg/m^3$, specific heat per unit mass $C_v = 420\,J/KgK$, coefficients of thermal expansion $\alpha_{11} = \alpha_{22} = 1.5 \times 10^{-6}\,K^{-1}$ and $\alpha_{33} = 2 \times 10^{-6}\,K^{-1}$, thermal conductivity coefficients $\kappa_{11} = \kappa_{22} = \kappa_{33} = 1.8\,W/mK$, pyroelectric constant $p_3 = 0.0007\,C/m^2K$, piezoelectric coefficients $e_{31} = e_{32} = -5.20\,C/m^2$, $e_{33} = 15.08\,C/m^2$ and $e_{15} = e_{24} = 12.72\,C/m^2$ and dielectric constants $\varepsilon_{11} = \varepsilon_{22} = 1.306 \times 10^{-8}\,F/m$ and $\varepsilon_{33} = 1.151 \times 10^{-8}\,F/m$.

The values in the Table 4 are displacements in $10^{-12}m$, stresses in $10^{-1}Pa$ and electric potential in V. The LD4(u, Φ, θ) gives a quasi-3D description in terms of the above variables, the results are not perfectly coincident with the 3D solution by Heyliger [45] because the thermal effect is considered in our model. If the thermal effect is not considered, as in the LD4(u, Φ), the results are perfectly coincident with the 3D ones. However the thermal effect is very small and it can be discarded. The values in the plate are given at both the top and bottom of the interface between the two fibre reinforced composite layers, and also at the top and bottom of the whole multilayered structure. A correct 3D analysis gives the continuity of the displacements and electric potential at the interface, the in-plane stresses can be discontinuous. The plate is very thick with high in-plane and transverse anisotropy, for this reason the use of ESL models such as the ED4(u, Φ, θ) one and classical theories (FSDT(u, Φ, θ) and CLT(u, Φ, θ)) is inadequate. These last theories give only good result for the electric potential, this happens because we have made the choice that the electric potential is in LW form in each considered model (with the same order of expansion employed for the other variables). The electric field effect cannot be discarded because models where the electric potential is a primary

Table 4 Second assessment: Electric potential applied to a multilayered composite plate with two external piezoelectric layers

	$v(0.5h)$	$v(0^{\pm})$	$v(-0.5h)$	$\sigma_{yy}(0.5h)$	$\sigma_{yy}(0^{\pm})$	$\sigma_{yy}(-0.5h)$
3D [45]	−32.764	0.0295	−2.8625	111.81	−1.3905	27.795
		0.0295			−1.3089	
LD4(u, Φ, θ)	−32.780	0.0297	−2.8547	111.21	−1.3946	27.728
		0.0297			−1.3105	
ED4(u, Φ, θ)	−37.737	−1.7618	−7.3165	238.36	18.437	120.53
		−1.7618			3.0676	
FSDT(u, Φ, θ)	−4.2243	−4.7287	−5.2331	−111.78	39.722	−83.795
		−4.7287			−9.8430	
CLT(u, Φ, θ)	−0.9327	−0.1732	0.5863	−19.587	2.0975	−8.7364
		−0.1732			0.4778	
LD4(u, Φ)	−32.765	0.0297	−2.8618	111.80	−1.3953	27.784
		0.0297			−1.3099	
	$\Phi(0.5h)$	$\Phi(0^{\pm})$	$\Phi(-0.5h)$			
3D [45]	1.0000	0.4476	0.0000			
		0.4476				
LD4(u, Φ, θ)	1.0000	0.4476	0.0000			
		0.4476				
ED4(u, Φ, θ)	1.0000	0.4481	0.0000			
		0.4481				
FSDT(u, Φ, θ)	1.0000	0.4461	0.0000			
		0.4461				
CLT(u, Φ, θ)	1.0000	0.4469	0.0000			
		0.4469				
LD4(u, Φ)	1.0000	0.4477	0.0000			
		0.4477				

Comparison between classical, refined and three-dimensional models for the thickness ratio $a/h = 4$. The dimensional values are the maximum amplitudes in the plane. Displacements are in $10^{-12}m$, stresses are in $10^{-1}Pa$ and electric potential is in V.

variable are mandatory, in fact this feature allows the electric voltage on the surfaces to be imposed. In this case the LD4(u,Φ,θ) model is very close to the 3D solution by Heyliger [45] even if the thermal effect is included and the plate is thick, this means that the model can be used as a reference solution in future benchmarks in the case of applied electric potential.

Third Assessment, Imposed Temperature

The simply supported plate has thickness ratio $S = a/h$ equals 5 with total thickness $h = 1\,m$. A sovra-temperature θ (referred to the room reference temperature T_0) is applied at the top surface in the form $\theta = \theta_t \sin(\frac{m\pi x}{a})$ with $\theta_t = 1\,K$ and wave numbers $m = 1$ and $n = 0$. The bottom of the plate has the sovra-temperature imposed to zero ($\theta_b = 0\,K$). In the case given by Vel [30] a thermo-mechanical analysis is proposed by means of a refined analytical model which gives a quasi-3D description. The plate has two layers made of a fiber reinforced Gr/Ep composite material, the lamination sequence is 0°/90° with thickness $h_1 = h_2 = 0.5\,h$. The employed material has Young modulii $E_1 = 200\,GPa$, $E_2 = 10\,GPa$ and $E_3 = 20\,GPa$, shear modulii $G_{12} = 7\,GPa$, $G_{13} = 5\,GPa$ and $G_{23} = 2\,GPa$, Poisson ratios $v_{12} = v_{13} = v_{23} = 0.3$, mass density $\rho = 1578\,Kg/m^3$, specific heat per unit mass $C_v = 1409\,J/KgK$, coefficients of thermal expansion $\alpha_{11} = 0.02 \times 10^{-6}\,K^{-1}$ and $\alpha_{22} = \alpha_{33} = 22.5 \times 10^{-6}\,K^{-1}$, thermal conductivity coefficients $\kappa_{11} = 1.5\,W/mK$, $\kappa_{22} = 0.5\,W/mK$ and $\kappa_{33} = 0.4\,W/mK$ and dielectric constants $\varepsilon_{11} = \varepsilon_{22} = \varepsilon_{33} = 1.53 \times 10^{-8}\,F/m$.

The results are given in terms of displacements and stresses in Table 5, displacements are in no-dimensional form via multiplication by the coefficient $AD1 = 1/(a\alpha_T T_0)$, stresses are in no-dimensional form via multiplication by

Table 5 Third assessment: Temperature imposed in a multilayered composite plate. Comparison between classical and refined models for the thickness ratio $a/h = 5$

	$\bar{u}(0.25a, -0.5h)$	$\bar{w}(0.5a, 0^{\pm})$	$\bar{\sigma}_{xx}(0.5a, 0.5h)$	$\bar{\sigma}_{xz}(0.25a, 0^{\pm})$	$\bar{\sigma}_{zz}(0.5a, 0^{\pm})$
Ref. [30]	0.0204	0.2976	−0.2160	−0.0392	0.0092
		0.2976		−0.0392	0.0092
LD4(u, Φ, θ)	0.0204	0.2976	−0.2161	−0.0392	0.0092
		0.2976		−0.0380	0.0094
ED4(u, Φ, θ)	0.0204	0.2972	−0.2218	−0.0122	0.0016
		0.2972		−0.0305	0.0177
LD1(u, Φ, θ)	0.0248	0.3218	−0.3008	−0.0331	0.3607
		0.3218		0.0319	−0.2990
ED2(u, Φ, θ)	0.0193	0.2909	−0.2366	−0.0067	0.0207
		0.2909		−0.0166	0.0373
FSDT(u, Φ, θ)	0.0389	0.3971	−0.4242	0.0026	\
		0.3971		0.0066	\
CLT(u, Φ, θ)	0.0397	0.4137	−0.4349	\	\
		0.4137		\	\
LD4(u, θ)	0.0204	0.2976	−0.2161	−0.0392	0.0092
		0.2976		−0.0380	0.0094

The non-dimensional values are in particular points in the plane. Cylindrical loads which mean that the only dimension a affects the results.

the coefficient $AD2 = 1/(\alpha_T E_T T_0)$ ($T_0 = 1\,K$, $a = 5\,m$, $\alpha_T = 22.5 \times 10^{-6}\,K$, $E_T = 20\,GPa$). In Table 5 the in-plane displacement is evaluated at the bottom of the plate, the normal in-plane stress is given at the top of the plate, transverse displacement and transverse shear/normal stresses are calculated at the interface between the two layers (both top and bottom of this interface). The plate is in cylindrical bending condition ($n = 0$), therefore the behavior in the y direction along the b side is not relevant. This proposed assessment is not a thermo-electro-mechanical problem, but it is a thermo-mechanical analysis, however we use it to validate our models when a temperature is imposed on the surfaces. There are no differences between LD4(u, Φ, θ) and LD4(u, θ) models because no electric field is generated in such a problem, therefore the electric field effect does not exist and LD4(u, Φ, θ) theory degenerates in the LD4(u, θ) one. The quasi-3D description of the problem (in particular for displacements and in-plane stresses) is obtained with a LW higher-order model, the transverse stresses are correctly evaluated even if small differences appear at the interface for the interlaminar continuity, however this problem will be easily solved in future works by means of mixed layer wise models.

In Table 5, it is clear how a LW model does not give the 3D solution when a low order of expansion is used through the thickness (see in particular the stress results). The use of ESL models is quite correct for the displacements but it is not correct for the stresses, in particular the transverse ones. Finally, ESL model with low order of expansion (ED2(u, Φ, θ)) and classical models such as FSDT(u, Φ, θ) and CLT(u, Φ, θ) ones are completely inadequate for the analysis of these multilayered structures. CLT does not give any result for transverse shear/normal stresses because they are zero as hypothesis in such a theory, the same happens for the FSDT, which has transverse normal stress σ_{zz} equals zero as hypothesis. The discussion of the results in Table 5 demonstrates how LW refined models can be used as a reference solution in future benchmarks in the case of applied temperature at the external surfaces.

Thermo-electro-mechanical Evaluation in Smart Plates

The multilayered smart plate employed for the benchmarks proposed in this section is a simply supported square plate ($a = b = 10\,m$) with thickness ratios $S = a/h = 10, 20, 100$ (which means total thickness h equals $1\,m$, $0.5\,m$ and $0.1\,m$, respectively). The structure has two layers of the same thickness $h_1 = h_2 = 0.5h$, the bottom layer is in graphite-epoxy material with fibre orientation 0°, the top layer is in piezoelectric material PZT. The composite material has Young modulii $E_1 = 144.23\,GPa$ and $E_2 = E_3 = 9.65\,GPa$, shear modulii $G_{12} = G_{13} = 4.14\,GPa$ and $G_{23} = 3.45\,GPa$, Poisson ratios $\nu_{12} = \nu_{13} = \nu_{23} = 0.3$, mass density $\rho = 1389.23\,Kg/m^3$, specific heat per unit mass $C_v = 1409\,J/KgK$, coefficients of thermal expansion $\alpha_{11} = 1.1 \times 10^{-6}\,K^{-1}$ and $\alpha_{22} = \alpha_{33} = 25.2 \times 10^{-6}\,K^{-1}$, thermal conductivity coefficients $\kappa_{11} = 4.48\,W/mK$ and $\kappa_{22} = \kappa_{33} = 3.21\,W/mK$ and dielectric constants $\varepsilon_{11} = 3.098966 \times 10^{-11}\,F/m$ and $\varepsilon_{22} = \varepsilon_{33} = 2.6562563 \times 10^{-11}\,F/m$.

The piezoelectric layer has Young modulii $E_1 = E_2 = E_2 = 63\,GPa$, Poisson ratios $\nu_{12} = \nu_{13} = \nu_{23} = 0.28$, mass density $\rho = 7600\,Kg/m^3$, specific heat per unit mass $C_v = 420\,J/KgK$, coefficients of thermal expansion $\alpha_{11} = \alpha_{22} = \alpha_{33} = 0.9 \times 10^{-6}\,K^{-1}$, thermal conductivity coefficients $\kappa_{11} = \kappa_{22} = \kappa_{33} = 2.1\,W/mK$, pyroelectric

constant $p_3 = 20 \times 10^{-6}\, C/m^2K$, piezoelectric coefficients $e_{31} = e_{32} = -5.20\, C/m^2$, $e_{33} = 15.08\, C/m^2$ and $e_{15} = e_{24} = 12.72\, C/m^2$ and dielectric constants $\varepsilon_{11} = \varepsilon_{22} = 15.3 \times 10^{-9}\, F/m$ and $\varepsilon_{33} = 15.0 \times 10^{-9}\, F/m$. The plate proposed is subjected to three different loadings as shown in Figure 2.

The first case considers a bi-sinusoidal mechanical pressure applied at the top surface with amplitude $p_t = 1\, Pa$ and wave numbers $m = n = 1$, the electric potential is set to zero at both top and bottom surfaces ($\Phi_t = \Phi_b = 0$) and the sovra-temperature is free. The second case considers a bi-sinusoidal electric voltage applied at the top of the plate with amplitude $\Phi_t = 1\, V$ and wave numbers $m = n = 1$, the bottom is set to zero ($\Phi_b = 0\, V$), the sovra-temperature is free at both top and bottom surfaces. The third and last case analyzes a plate with imposed bi-sinusoidal sovra-temperature at the top surface with amplitude $\theta_t = 1\, K$ and wave numbers $m = n = 1$. The bottom surface has a zero imposed sovra-temperature, the electric potential is free considered at both the top and bottom of the plate.

The benchmark with applied mechanical load is investigated in Tables 6–8 and in Figures 3 and 4. In Table 6 a moderately thick plate is investigated, the LD4(u, Φ, θ) gives a transverse displacement which considers both the electrical and thermal field effects, therefore such a model is able to obtain both the sovra-temperature and the electric potential directly from the governing equations (they are primary variables as the displacements), the stresses and the electric displacement are correctly obtained from the constitutive equations via

Table 6 Benchmark: Mechanical load applied to a thick ($a/h = 10$) smart plate

	$w(0)$	$\theta(0)$	$\Phi(0)$	$\sigma_{xz}(0.25h)$	$\sigma_{xx}(0.5h)$	$\mathscr{D}_z(0.25h)$
LD4(u, Φ, θ)	0.7955×10^{-8}	0.3324×10^{-8}	0.0522	2.6807	35.043	0.1205×10^{-9}
ED4(u, Φ, θ)	0.7756×10^{-8}	0.3562×10^{-8}	0.0535	1.3075	34.786	0.2017×10^{-9}
FSDT(u, Φ, θ)	0.7087×10^{-8}	0.4839×10^{-8}	0.0434	3.8514	34.197	0.1927×10^{-9}
CLT(u, Φ, θ)	0.6666×10^{-8}	-0.7319×10^{-8}	0.0276	\	34.461	-0.1538×10^{-10}
LD4(u, Φ)	0.7956×10^{-8}	\	0.0522	2.6809	35.047	0.1205×10^{-9}
LD4(u, θ)	0.8258×10^{-8}	0.2870×10^{-8}	\	2.6356	32.790	\
LD4(u)	0.8260×10^{-8}	\	\	2.6359	32.794	\

Thermo-electro-mechanical variables evaluated by means of classical and refined two-dimensional models. The dimensional values are the maximum amplitudes in the plane.

Table 7 Benchmark: Mechanical load applied to a moderately thick ($a/h = 20$) smart plate

	$w(0)$	$\theta(0)$	$\Phi(0)$	$\sigma_{xz}(0.25h)$	$\sigma_{xx}(0.5h)$	$\mathscr{D}_z(0.25h)$
LD4(u, Φ, θ)	0.5820×10^{-7}	0.1356×10^{-7}	0.1085	5.2737	135.69	0.1088×10^{-9}
ED4(u, Φ, θ)	0.5779×10^{-7}	0.1358×10^{-7}	0.1091	2.4463	135.51	0.1928×10^{-9}
FSDT(u, Φ, θ)	0.5435×10^{-7}	0.1962×10^{-7}	0.0849	7.7273	136.99	0.1867×10^{-9}
CLT(u, Φ, θ)	0.5332×10^{-7}	-0.2925×10^{-7}	0.0559	\	137.85	-0.2002×10^{-10}
LD4(u, Φ)	0.5822×10^{-7}	\	0.1085	5.2742	135.70	0.1088×10^{-9}
LD4(u, θ)	0.6039×10^{-7}	0.1195×10^{-7}	\	5.1903	127.19	\
LD4(u)	0.6040×10^{-7}	\	\	5.1909	127.21	\

Thermo-electro-mechanical variables evaluated by means of classical and refined two-dimensional models. The dimensional values are the maximum amplitudes in the plane.

Table 8 Benchmark: Mechanical load applied to a thin ($a/h = 100$) smart plate

	$w(0)$	$\theta(0)$	$\Phi(0)$	$\sigma_{xz}(0.25h)$	$\sigma_{xx}(0.5h)$	$\mathscr{D}_z(0.25h)$
LD4(u, Φ, θ)	0.7050×10^{-5}	0.3412×10^{-6}	0.5496	26.221	3355.0	-0.1722×10^{-9}
ED4(u, Φ, θ)	0.7048×10^{-5}	0.3337×10^{-6}	0.5487	11.948	3357.9	-0.8679×10^{-10}
FSDT(u, Φ, θ)	0.6699×10^{-5}	0.4925×10^{-6}	0.4213	38.676	3426.4	-0.2788×10^{-10}
CLT(u, Φ, θ)	0.6665×10^{-5}	-0.7311×10^{-6}	0.2805	\	3446.2	-0.1631×10^{-9}
LD4(u, Φ)	0.7051×10^{-5}	\	0.5495	26.224	3355.4	-0.1726×10^{-9}
LD4(u, θ)	0.7314×10^{-5}	0.3026×10^{-6}	\	25.816	3147.1	\
LD4(u)	0.7315×10^{-5}	\	\	25.819	3147.5	\

Thermo-electro-mechanical variables evaluated by means of classical and refined two-dimensional models. The dimensional values are the maximum amplitudes in the plane.

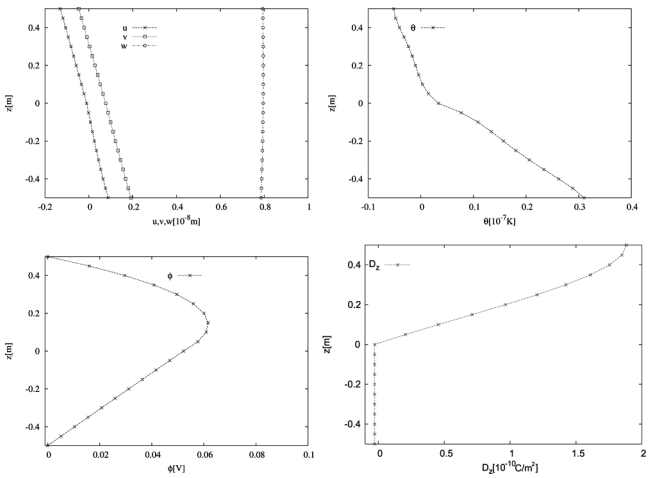

Figure 3 Benchmark: Mechanical load applied to a moderately thick ($a/h = 10$) smart plate. Thermo-electro-mechanical variables through the thickness z via LD4(u, Φ, θ) model.

a post-processing because the primary variables are correctly calculated. If we consider the ESL models and the classical ones (ED4(u, Φ, θ), FSDT(u, Φ, θ), CLT(u, Φ, θ)) including the multifield effects, some problems appear, in particular classical models are completely inadequate.

The LD4(u, Φ) discards the thermal effect and this demonstrates as the thermal field is not important in such a problem, however this model is not able to give information about the temperature field. The LD4(u, θ) discards the electric field, in this case the electric field effect is much more important than the thermal field effect, moreover no information about the electric potential and the electric displacement can be obtained. The LD4(u) discards both the electric and thermal fields, when a physical field is discarded the transverse displacement is bigger because there is not conversion from the energy given by the load to the electric and/or thermal energy. The LD4(u) does not give any information about the electric and thermal variables. Figure 3 shows the displacements, the sovra-temperature, the electric potential and the electric displacement through the thickness of the

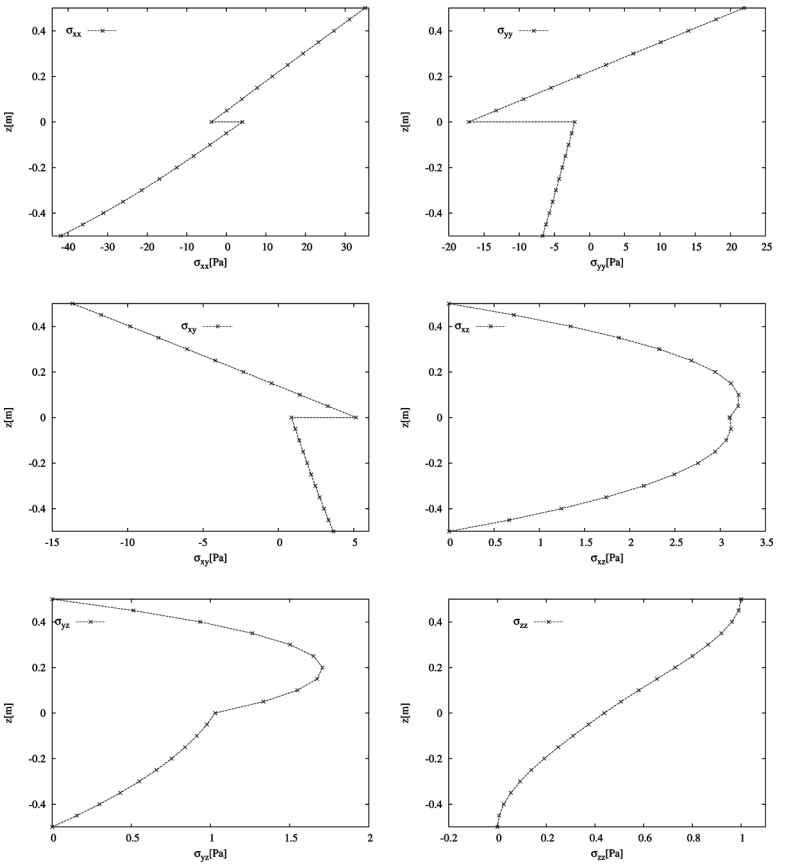

Figure 4 Benchmark: Mechanical load applied to a moderately thick ($a/h = 10$) smart plate. Thermo-electro-mechanical stresses through the thickness z via LD4(u, Φ, θ) model.

moderately thick plate, the employed theory is the LD4(u, Φ, θ), this last also gives a correct 3D description of the stresses through the thickness of the moderately thick plate (see Figure 4). The plate is in bending, therefore the bottom part of the plate is in compression and the top part of the plate is in dilation, this means that the sovra-temperature is positive for the bottom part and negative for the top part. It is obvious that such temperature values are very small because the effect is unimportant. The electric potential through the thickness confirms the boundary conditions imposed ($\Phi_t = \Phi_b = 0\,V$).

The transverse shear stresses and the transverse normal stress in Figure 4 confirms the correct evaluation of such a variables and the loading conditions: zero transverse shear stresses at the top and bottom of the plate, transverse normal stress equals $1\,Pa$ at the top where the load is applied and zero at the bottom of the plate. The normal and shear in-plane stresses are also correctly evaluated through the thickness and the typical discontinuity at the interface is shown. Tables 7 and 8 propose the same results already discussed for the thick plate in the case of smaller thickness, the conclusions and discussion are almost the same: the multifield effects

given by the thermal and electrical fields appear as independent on the thickness value of the plate. The results given by the ED4(u, Φ, θ) looks more correct than the thick plate case but the use of classical theories remains inadequate.

The benchmark with applied electric potential is investigated in Tables 9–11 and in Figures 5 and 6. A moderately thick plate is investigated in Table 9, the LD4(u, Φ, θ) gives a transverse displacement which considers the multifield effects, therefore such a model permits to obtain the displacements, the sovra-temperature and the electric potential directly from the governing equations, the stresses and the electric displacement are correctly obtained via post-processing by using constitutive equations. ESL models and the classical ones (ED4(u, Φ, θ), FSDT(u, Φ, θ), CLT(u, Φ, θ)) including the multifield effects exhibit some problems; in particular classical models are completely inadequate. In this case LD4(u, θ) and LD4(u) cannot be used because the electric field cannot be discarded, it permits

Table 9 Benchmark: Electric potential applied to a thick ($a/h = 10$) smart plate

	$w(0)$	$\theta(0)$	$\Phi(0)$	$\sigma_{xz}(0.25h)$	$\sigma_{xx}(0.5h)$	$\mathscr{D}_z(0.25h)$
LD4(u, Φ, θ)	-0.1812×10^{-9}	0.1522×10^{-9}	0.9717	0.0178	-0.1090	-0.1104×10^{-8}
ED4(u, Φ, θ)	-0.2341×10^{-9}	0.1143×10^{-9}	0.9723	-0.2783	-0.2354	-0.1078×10^{-8}
FSDT(u, Φ, θ)	-0.3902×10^{-9}	0.2761×10^{-9}	0.9727	0.5548	-0.1738	-0.1071×10^{-8}
CLT(u, Φ, θ)	0.2232×10^{-10}	0.2583×10^{-10}	0.9740	\	-0.0486	-0.7946×10^{-9}
LD4(u, Φ)	-0.1812×10^{-9}	\	0.9717	0.0178	-0.1090	-0.1104×10^{-8}

Thermo-electro-mechanical variables evaluated by means of classical and refined two-dimensional models. The dimensional values are the maximum amplitudes in the plane.

Table 10 Benchmark: Electric potential applied to a moderately thick ($a/h = 20$) smart plate

	$w(0)$	$\theta(0)$	$\Phi(0)$	$\sigma_{xz}(0.25h)$	$\sigma_{xx}(0.5h)$	$\mathscr{D}_z(0.25h)$
LD4(u, Φ, θ)	-0.1717×10^{-9}	0.8100×10^{-10}	0.9918	0.0047	-0.0600	-0.6416×10^{-9}
ED4(u, Φ, θ)	-0.2274×10^{-9}	0.7292×10^{-10}	0.9919	-0.3023	-0.1235	-0.6282×10^{-9}
FSDT(u, Φ, θ)	-0.3888×10^{-9}	0.1578×10^{-9}	0.9920	0.5696	-0.0999	-0.6214×10^{-9}
CLT(u, Φ, θ)	0.2705×10^{-10}	0.1534×10^{-10}	0.9921	\	-0.0294	-0.4814×10^{-9}
LD4(u, Φ)	-0.1717×10^{-9}	\	0.9918	0.0047	-0.0600	-0.6416×10^{-9}

Thermo-electro-mechanical variables evaluated by means of classical and refined two-dimensional models. The dimensional values are the maximum amplitudes in the plane.

Table 11 Benchmark: Electric potential applied to a thin ($a/h = 100$) smart plate

	$w(0)$	$\theta(0)$	$\Phi(0)$	$\sigma_{xz}(0.25h)$	$\sigma_{xx}(0.5h)$	$\mathscr{D}_z(0.25h)$
LD4(u, Φ, θ)	0.1091×10^{-9}	0.3904×10^{-10}	0.9984	0.2720×10^{-3}	-0.0780	-0.6383×10^{-9}
ED4(u, Φ, θ)	0.5191×10^{-10}	0.1038×10^{-9}	0.9984	-0.3104	-0.0716	-0.6356×10^{-9}
FSDT(u, Φ, θ)	-0.1757×10^{-9}	0.1462×10^{-9}	0.9983	0.5745	-0.0945	-0.6340×10^{-9}
CLT(u, Φ, θ)	0.1702×10^{-9}	0.1775×10^{-10}	0.9980	\	-0.0370	-0.6057×10^{-9}
LD4(u, Φ)	0.1091×10^{-9}	\	0.9984	0.2720×10^{-3}	-0.0780	-0.6383×10^{-9}

Thermo-electro-mechanical variables evaluated by means of classical and refined two-dimensional models. The dimensional values are the maximum amplitudes in the plane.

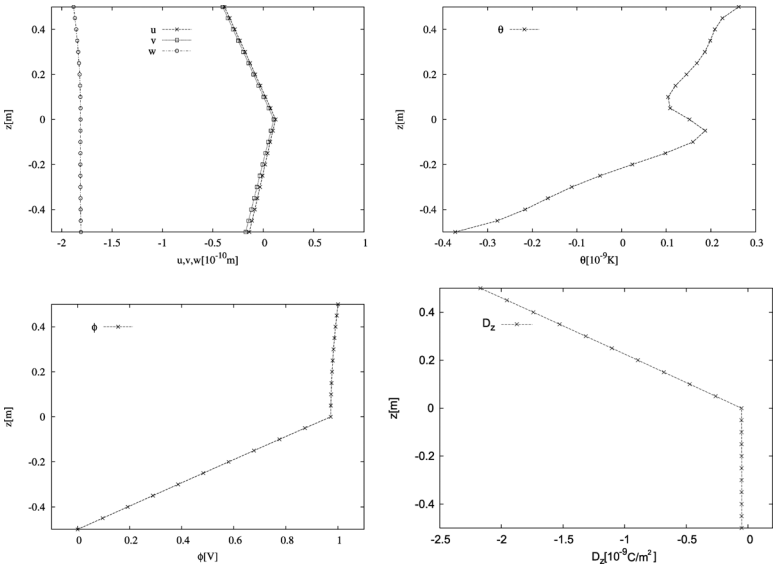

Figure 5 Benchmark: Electric potential applied to a moderately thick ($a/h = 10$) smart plate. Thermo-electro-mechanical variables through the thickness z via LD4(u, Φ, θ) model.

to impose the electric voltage and to evaluate its effects in such a smart structure. On the contrary, the results for the LD4(u, Φ) are given because this model allows the electric voltage to be imposed and the thermal field effects to be evaluated: the results do not change in such a case even if the informations about the thermal field are discarded. Figure 5 shows the displacements, the sovra-temperature, the electric potential and the electric displacement through the thickness of the moderately thick plate, the employed theory is the LD4(u, Φ, θ), this last also gives a correct 3D description of the stresses through the thickness of the moderately thick plate (see Figure 6). The sovra-temperature through the thickness due to the electric load is very small (order of $10^{-9}\,K$) and the electric potential correctly includes the loading conditions ($1\,V$ applied at the top and $0\,V$ imposed at the bottom). The stresses are correctly evaluated in a quasi-3D form, the in-plane stresses show the discontinuity at the interface while the transverse shear and normal stresses satisfy the loading conditions which are zero values at the top and bottom surfaces because no mechanical loads have been applied. Tables 10 and 11 propose the same results already discussed for the thick plate in the case of smaller thickness, the multifield effects are independent on the thickness value of the plate. Each theory different from the LW ones with higher orders of expansion is inappropriate to investigate such a problem even when the thickness is smaller (field loads are more complicated than mechanical loads in the first part of this section).

The benchmark with imposed sovra-temperature at the top of the plate is investigated in Tables 12–14 and in Figures 7 and 8. A moderately thick plate is investigated in Table 12, the LD4(u, Φ, θ) gives a transverse displacement which considers the multifield effects, and it allows the displacements, the sovra-temperature and the electric potential to be directly obtained from the governing equations; the stresses and the electric displacement are correctly obtained via a

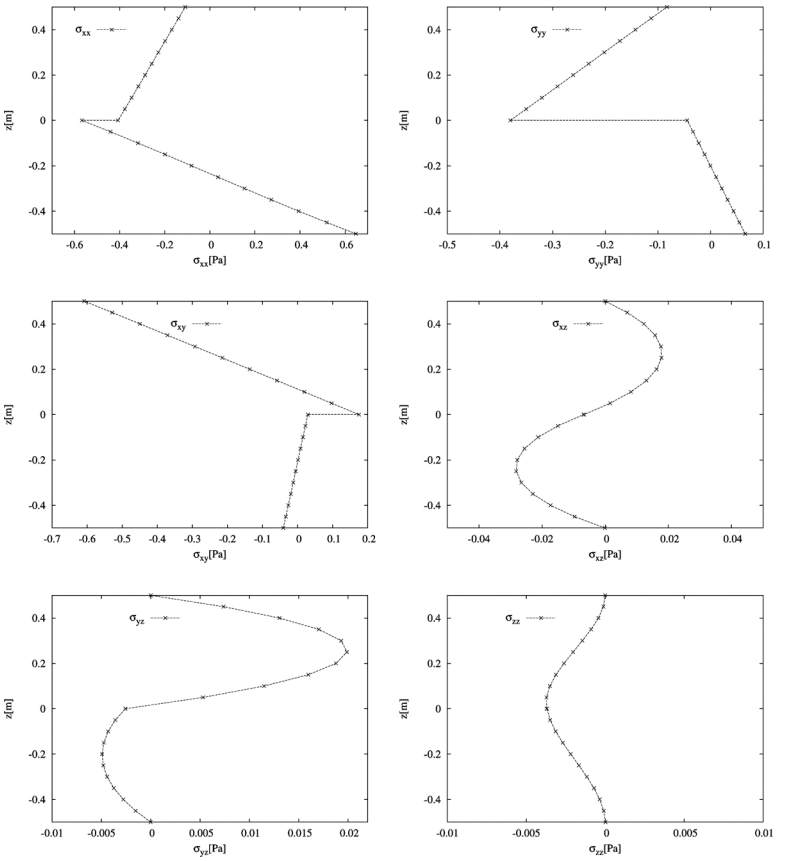

Figure 6 Benchmark: Electric potential applied to a moderately thick ($a/h = 10$) smart plate. Thermo-electro-mechanical stresses through the thickness z via LD4(u, Φ, θ) model.

post-processing. ESL models and the classical ones (ED4(u, Φ, θ), FSDT(u, Φ, θ), CLT(u, Φ, θ)) including the multifield effects, are completely inadequate for the investigation of such a problem. LD4(u, Φ) and LD4(u) cannot be considered because the thermal field cannot be discarded, it permits us to impose the

Table 12 Benchmark: Temperature imposed to a thick ($a/h = 10$) smart plate

	$w(0)$	$\theta(0)$	$\Phi(0)$	$\sigma_{xz}(0.25h)$	$\sigma_{xx}(0.5h)$	$\mathscr{D}_z(0.25h)$
LD4(u, Φ, θ)	-0.6547×10^{-6}	0.3852	−165.34	−1583.6	−65449	0.1773×10^{-6}
ED4(u, Φ, θ)	-0.1220×10^{-5}	0.3852	−297.67	−604.95	−27087	0.1705×10^{-6}
FSDT(u, Φ, θ)	-0.5254×10^{-5}	0.3851	−348.55	−2376.0	−77357	0.4566×10^{-7}
CLT(u, Φ, θ)	-0.5198×10^{-5}	0.3851	−355.07	\	−77106	0.4720×10^{-7}
LD4(u, θ)	-0.2312×10^{-5}	0.3852	\	−1455.1	−56319	\

Thermo-electro-mechanical variables evaluated by means of classical and refined two-dimensional models. The dimensional values are the maximum amplitudes in the plane.

Table 13 Benchmark: Temperature imposed to a moderately thick ($a/h = 20$) smart plate

	$w(0)$	$\theta(0)$	$\Phi(0)$	$\sigma_{xz}(0.25h)$	$\sigma_{xx}(0.5h)$	$\mathscr{D}_z(0.25h)$
LD4(u, Φ, θ)	-0.2320×10^{-5}	0.3929	−84.324	−849.88	−67376	0.4504×10^{-7}
ED4(u, Φ, θ)	-0.2734×10^{-5}	0.3929	−151.62	−315.75	−27266	0.4326×10^{-7}
FSDT(u, Φ, θ)	-0.1051×10^{-4}	0.3929	−176.70	−1242.4	−78071	0.1155×10^{-7}
CLT(u, Φ, θ)	-0.1064×10^{-4}	0.3929	−179.86	\	−77525	0.1030×10^{-7}
LD4(u, θ)	-0.5569×10^{-5}	0.3929	\	−783.61	−58148	\

Thermo-electro-mechanical variables evaluated by means of classical and refined two-dimensional models. The dimensional values are the maximum amplitudes in the plane.

Table 14 Benchmark: Temperature imposed to a thin ($a/h = 100$) smart plate

	$w(0)$	$\theta(0)$	$\Phi(0)$	$\sigma_{xz}(0.25h)$	$\sigma_{xx}(0.5h)$	$\mathscr{D}_z(0.25h)$
LD4(u, Φ, θ)	-0.1325×10^{-4}	0.3954	−16.973	−173.87	−68018	0.1811×10^{-8}
ED4(u, Φ, θ)	-0.1413×10^{-4}	0.3954	−30.504	−63.981	−27326	0.1739×10^{-8}
FSDT(u, Φ, θ)	-0.5254×10^{-4}	0.3954	−35.498	−252.07	−78307	0.4638×10^{-9}
CLT(u, Φ, θ)	-0.5361×10^{-4}	0.3954	−36.122	\	−77661	0.4791×10^{-9}
LD4(u, θ)	-0.2938×10^{-4}	0.3954	\	−160.48	−58758	\

Thermo-electro-mechanical variables evaluated by means of classical and refined two-dimensional models. The dimensional values are the maximum amplitudes in the plane.

sovra-temperature and to evaluate its effects in such a structure. The LD4(u, θ) results are proposed because this model permits to impose the sovra-temperature and to evaluate the electric field effects, these last are very important. The electric field effect is noteworthy in a smart structure subjected to thermal loads. Figure 7

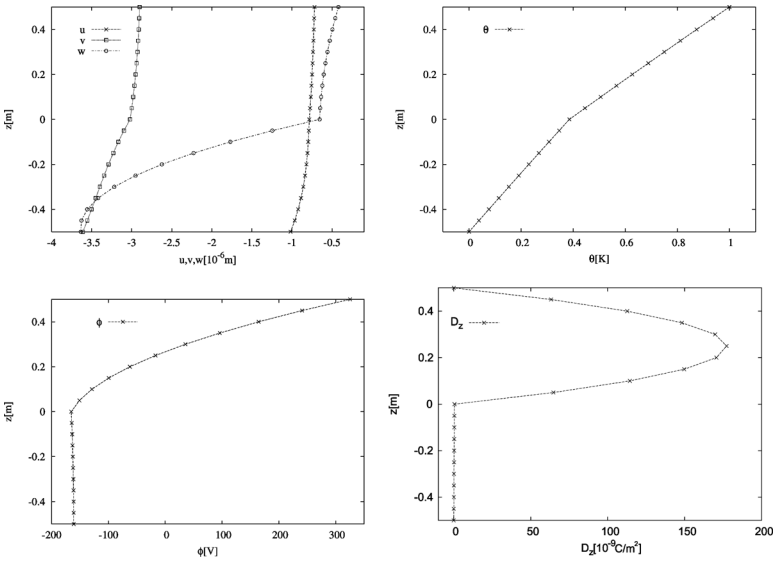

Figure 7 Benchmark: Temperature imposed to a moderately thick ($a/h = 10$) smart plate. Thermo-electro-mechanical variables through the thickness z via LD4(u, Φ, θ) model.

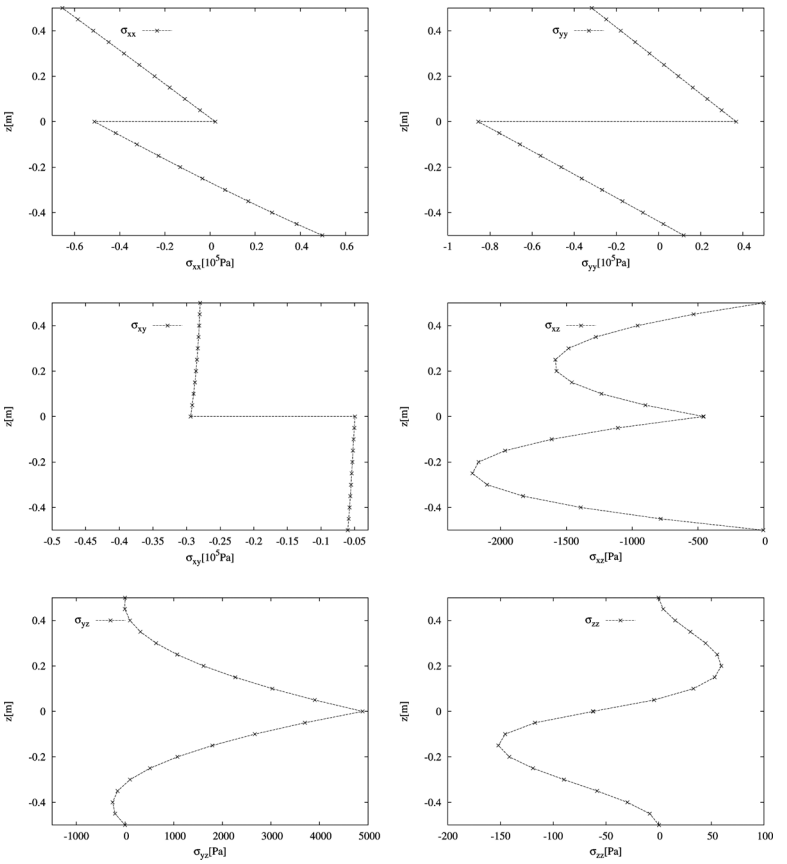

Figure 8 Benchmark: Temperature imposed to a moderately thick ($a/h = 10$) smart plate. Thermo-electro-mechanical stresses through the thickness z via LD4(u, Φ, θ) model.

shows the displacements, the sovra-temperature, the electric potential and the electric displacement through the thickness of the moderately thick plate, the employed theory is the LD4(u, Φ, θ), this last also gives a correct 3D description of the stresses through the thickness of the moderately thick plate (see Figure 8).

The sovra-temperature through the thickness confirms the load conditions which are $\theta_t = 1\,K$ at the top and $\theta_b = 0\,K$ at the bottom. The electric potential and the electric displacement are significant through the thickness of the plate and this confirms the importance of the electric field in such a problem. The stresses are correctly evaluated, the in-plane stresses show the discontinuity at the interface, yet the transverse shear and normal stresses satisfy the loading conditions, which are zero values at the top and bottom surfaces because no mechanical loads have been applied. Tables 13 and 14 discuss the effect of the thickness for the $a/h = 20$ and $a/h = 100$ cases: the results of the ED4(u, Φ, θ) model are more refined if compared with the thick case, the use of the classical models remains inadequate even if the plate is thin. From the analysis of the LD4(u, θ) results, it is clear how the thickness has not effect on the multifield coupling.

CONCLUSIONS

This paper has analyzed the static response of multilayered smart plates embedding piezoelectric layers in the case of mechanical loads, imposed electric potential and imposed sovra-temperature. The proposed multifield models consider the mechanical, electric and thermal field effects and their coupling. The refined kinematics based on a layer wise approach give a quasi-3D description of such problems in terms of each mechanical, thermal and electrical variable. It has been demonstrated how the use of classical models based on the extension of Kirchhoff and Reissner-Mindlin models to multifield problems is completely inadequate for the cases proposed, the ESL models with higher orders of expansion improve the results but they could not be appropriate for some cases. This means that the use of LW models, where the electro-thermo-mechanical variables have an higher order of expansion through the thickness, are mandatory for the multifield static investigation of piezoelectric plates. When a mechanical load is applied to a multilayered smart structure, the electric field effect is much more important than the thermal one, in the case of applied voltage the thermal field can be completely discarded, finally, for the case of imposed sovra-temperature on a smart structure the effect of the electric field is very important and it cannot be discarded. All these multifield effects do not depend on the thickness of the plate considered.

REFERENCES

1. E. Carrera, S. Brischetto, and P. Nali, Variational Statements and Computational Models for Multifiled Problems and Multilayered Structures, *Mech. Advan. Mat. Struct.*, vol. 15, pp. 182–198, 2008.
2. E. Carrera, S. Brischetto, and P. Nali, *Plates and Shells for Smart Structures: Classical and Advanced Theories for Modeling and Analysis*, John Wiley & Sons Ltd, New Delhi, 2011.
3. S. Brischetto and E. Carrera, Coupled Thermo-Mechanical Analysis of One-Layered and Multilayered Plates, *Compos. Struct.*, vol. 92, pp. 1793–1812, 2010.
4. J. L. Nowinski, *Theory of Thermoelasticity with Applications*, Sijthoff & Noordhoff, The Netherlands, 1978.
5. E. Carrera, S. Brischetto, and M. Cinefra, Variable Kinematics and Advanced Variational Statements for Free Vibrations Analysis of Piezoelectric Plates and Shells, *Comput. Mod. Eng. Sci.*, vol. 65, pp. 259–342, 2010.
6. E. Carrera and S. Brischetto, Piezoelectric Shell Theories with "A Priori" Continuous Transverse Electro-Mechanical Variables, *J. Mech. Mat. Struct.*, vol. 2, pp. 377–399, 2007.
7. G. A. Altay and M. C. Dökmeci, Fundamental Variational Equations of Discontinuous Thermopiezoelectric Fields, *Int. J. Eng. Sci.*, vol. 34, pp. 769–782, 1996.
8. G. A. Altay and M. C. Dökmeci, Some Variational Principles for Linear Coupled Thermoelasticity, *Int. J. Solids Struct.*, vol. 33, pp. 3937–3948, 1996.
9. A. A. Cannarozzi and F. Ubertini, A Mixed Variational Method for Linear Coupled Thermoelastic Analyis, *Int. J. Solids Struct.*, vol. 38, pp. 717–739, 2001.
10. G. Kirchhoff, Über Das Dleichgewicht und Die Bewegung Einer Elastishen Scheibe, *J. Reine Angew. Math*, vol. 40, pp. 51–88, 1850.
11. E. Reissner, The Effect of Transverse Shear Deformation on the Bending of Elastic Plates, *J. Appl. Mech.-T. ASME*, vol. 12, pp. 69–77, 1945.

12. R. D. Mindlin, Influence of Rotatory Inertia and Shear in Flexural Motions of Isotropic Elastic Plates, *J. Appl. Mech.-T. ASME*, vol. 18, pp. 31–38, 1951.
13. W. Q. Chen, K. Y. Lee, and H. J. Ding, General Solution for Transversely Isotropic Magneto-Electro-Thermo-Elasticity and the Potential Theory Method, *Int. J. Eng. Sci.*, vol. 42, pp. 1361–1379, 2004.
14. L. D. Pérez-Fernández, J. Bravo-Castillero, R. Rodríguez-Ramos and F.J. Sabina, On the Constitutive Relations and Energy Potentials of Linear Thermo-Magneto-Electro-Elasticity, *Mech. Res. Commun.*, vol. 36, pp. 343–350, 2009.
15. Y.-H. Liu and H.-M. Zhang, Variation Principle of Piezothermoelastic Bodies, Canonical Equation and Homogeneous Equation, *Appl. Math. Mech.*, vol. 28, pp. 193–200, 2007.
16. S.-J. Kim, A Constitutive Model for Thermo-Electro-Mechanical Behavior of Ferroelectric Polycrystals Near Room Temperature, *Int. J. Solids Struct.*, vol. 48, pp. 1318–1329, 2011.
17. A. Kumar and D. Chakraborty, Effective Properties of Thermo-Electro-Mechanically Coupled Piezoelectric Fiber Reinforced Composites, *Mater. Design*, vol. 30, pp. 1216–1222, 2009.
18. M. Sakthivel and A. Arockiarajan, An Analytical Model for Predicting Thermo-Electro-Mechanical Response of 1-3 Piezoelectric Composites, *Comp. Mater. Sci.*, vol. 48, pp. 759–767, 2010.
19. M. Sakthivel and A. Arockiarajan, Thermo-Electro-Mechanical Response of 1-3-2 Type Piezoelectric Composites, *Smart Mater. Struct.*, vol. 19, pp. 1–12, 2010.
20. Q.-S. Yang, Q.-H. Qin, L.-H. Ma, X.-Z. Lu, and C.-Q. Cui, A Theoretical Model and Finite Element Formulation for Coupled Thermo-Electro-Chemo-Mechanical Media, *Mech. Mater.*, vol. 42, pp. 148–156, 2010.
21. Y. T. Zhou and K. Y. Lee, Thermo-Electro-Mechanical Contact Behavior of a Finite Piezoelectric Layer Under a Sliding Punch with Frictional Heat Generation, *J. Mech. Phys. Solids*, vol. 59, pp. 1037–1061, 2011.
22. G. P. Dube, S. Kapuria, and P. C. Dumir, Exact Piezothermoleastic Solution of Simply-Supported Orthotropic Flat Panel in Cylindrical Bending, *Int. J. Mech. Sci.*, vol. 38, pp. 1161–1177, 1996.
23. C. Zhang, Y. K. Cheung, S. Di, and N. Zhang, The Exact Solution of Coupled Thermoelectroelastic Behavior of Piezoelectric Laminates, *Comput. Struct.*, vol. 80, pp. 1201–1212, 2002.
24. C. Zhang, S. Di, and N. Zhang, A New Procedure for Static Analysis of Thermo-Electric Laminated Composite Plates Under Cylindrical Bending, *Compos. Struct.*, vol. 56, pp. 131–140, 2002.
25. S. Kapuria and P. G. Nair, Exact Three-Dimensional Piezothermoelasticity Solution for Dynamics of Rectangular Cross-Ply Hybrid Plates Featuring Interlaminar Bonding Imperfections, *Compos. Sci. Technol.*, vol. 70, pp. 752–762, 2010.
26. K. Xu, A. K. Noor, and Y. Y. Tang, Three-Dimensional Solutions for Coupled Thermoelectroelastic Response of Multilayered Plates, *Comput. Method. Appl. M.*, vol. 126, pp. 355–371, 1995.
27. M. Cho and J. Oh, Higher Order Zig-Zag Theory for Fully Coupled Thermo-Electric-Mechanical Smart Composite Plates, *Int. J. Solids Struct.*, vol. 41, pp. 1331–1356, 2004.
28. M. Krommer, On the Influence of Pyroelectricity Upon Thermally Induced Vibrations of Piezothermoelastic Plates, *Acta Mech.*, vol. 171, pp. 59–73, 2004.
29. J. Oh, M. Cho and J.-S. Kim, Enhanced Lower-Order Shear Deformation Theory for Fully Coupled Electro-Thermomechanical Smart Laminated Plates, *Smart Mater. Struct.*, vol. 16, pp. 2229–2241, 2007.

30. S. S. Vel, Analytical Solutions for the Deformation of Anisotropic Elastic and Piezothermoelastic Laminated Plates, Ph.D. Dissertation, Virginia Polytechnic Institute and State University, Blacksburg, Virginia (USA), 1998.
31. H. J. Xiang, and Z. F. Shi, Static Analysis for Functionally Graded Piezoelectric Actuators or Sensors Under a Combined Electro-Thermal Load, *Eur. J. Mech. A-SOLID*, vol. 28, pp. 338–346, 2009.
32. S. Kapuria, A. Ahmed, and P. C. Dumir, Static and Dynamic Thermo-Electro-Mechanical Analysis of Angle-Ply Hybrid Piezoelectric Beams Using an Efficient Coupled Zigzag Theory, *Compos. Sci. Technol.*, vol. 64, pp. 2463–2475, 2004.
33. K. M. Liew, J. Z. Zhang, C. Li, and S. A. Meguid, Three-Dimensional Analysis of the Coupled Thermo-Piezoelectro-Mechanical Behaviour of Multilayered Plates Using the Differential Quadrature Technique, *Int. J. Solids Struct.*, vol. 42, pp. 4239–4257, 2005.
34. H.-S. Shen, Nonlinear Bending Analysis of Unsymmetric Cross-Ply Laminated Plates with Piezoelectric Actuators in Thermal Environments, *Compos. Struct.*, vol. 63, pp. 167–177, 2004.
35. J. Yang, S. Kitipornchai, and K. M. Liew, Large Amplitude Vibration of Thermo-Electro-Mechanically Stressed FGM Laminated Plates, *Comput. Method. Appl.*, vol. 192, pp. 3861–3885, 2003.
36. J. Yang, and H. J. Xiang, Thermo-Electro-Mechanical Characteristics of Functionally Graded Piezoelectric Actuators, *Smart Mater. Struct.*, vol. 16, pp. 784–797, 2007.
37. F. Côté, P. Masson, N. Mrad, and V. Cotoni, Dynamic and Static Modelling of Piezoelectric Composite Structures Using a Thermal Analogy with MSC/NASTRAN, *Compos. Struct.*, vol. 65, pp. 471–484, 2004.
38. G. Giannopoulos and J. Vantomme, A Thermal-Electrical-Mechanical Coupled FE Formulation Using Discrete Layer Kinematics for the Dynamic Analysis of Smart Plates, *Smart Mater. Struct.*, vol. 15, pp. 1846–1857, 2006.
39. H. Gu, A. Chattopadhyay, J. Li, and X. Zhou, A Higher Order Temperature Theory for Coupled Thermo-Piezoelectric-Mechanical Modeling of Smart Composites, *Int. J. Solids Struct.*, vol. 37, pp. 6479–6497, 2000.
40. H.-J. Lee and D. A. Saravanos, Generalized Finite Element Formulation for Smart Multilayered Thermal Piezoelectric Composite Plates, *Int. J. Solids Struct.*, vol. 34, pp. 3355–3371, 1997.
41. J. Oh and M. Cho, A Finite Element Based on Cubic Zig-Zag Plate Theory for the Prediction of Thermo-Electric-Mechanical Behaviors, *Int. J. Solids Struct.*, vol. 41, pp. 1357–1375, 2004.
42. K. D. Jonnalagadda, G. E. Blandford, and T. R. Tauchert, Piezothermoelastic Composite Plate Analysis Using First-Order Shear Deformation Theory, *Comput. Struct.*, vol. 51, pp. 79–89, 1992.
43. A. W. Leissa, *Vibration of Plates*, Report NASA SP-160, Washington, DC, USA, 1969.
44. J. N. Reddy, Mechanics of Laminated Composite Plates and Shells. *Theory and Analysis*, CRC Press, Boca Raton, USA, 2004.
45. P. Heyliger, Exact Solutions for Simply Supported Laminated Piezoelectric Plates, *J. Appl. Mech.-T. ASME*, vol. 64, pp. 299–306, 1997.